JCI insight

ANGPTL4 influences the therapeutic response of neovascular age-related macular degeneration patients by promoting choroidal neovascularization

Yu Qin, … , Silvia Montaner, Akrit Sodhi

JCI Insight. 2022. https://doi.org/10.1172/jci.insight.157896.

Research In-Press Preview **Ophthalmology**

Most patients with neovascular age-related macular degeneration (nvAMD), the leading cause of severe vision loss in elderly Americans, respond inadequately to current therapies targeting a single angiogenic mediator, vascular endothelial growth factor (VEGF). Here we report that aqueous levels of a second vasoactive mediator, angiopoietin-like 4 (ANGPTL4), can help predict the response of nvAMD patients to anti-VEGF therapies. ANGPTL4 expression was higher in patients who required monthly treatment with anti-VEGF therapies compared to patients who could be effectively treated with less frequent injections. We further demonstrate that ANGPTL4 acts synergistically with VEGF to promote the growth and leakage of choroidal neovascular (CNV) lesions in mice. Targeting ANGPTL4 expression was as effective as targeting VEGF expression for treating CNV in mice, while simultaneously targeting both was more effective than targeting either factor alone. To help translate these findings to patients, we used a soluble receptor that binds to both VEGF and ANGPTL4 and effectively inhibited the development of CNV lesions in mice. Our findings provide an assay that can help predict the response of nvAMD patients to anti-VEGF monotherapy and suggest that therapies targeting both ANGPTL4 and VEGF will be a more effective approach for the treatment of this blinding disease.

ANGPTL4 Influences the Therapeutic Response of Neovascular Age-Related Macular Degeneration Patients by Promoting Choroidal Neovascularization

Yu Qin[1,2], Aumreetam Dinabandhu[1,3], Xuan Cao[1], Jaron Castillo Sanchez[1], Kathleen Jee[1], Murilo Rodrigues[1], Chuanyu Guo[1], Jing Zhang[1,4], Jordan Vancel[1], Deepak Menon[3], Noore-Sabah Khan[1], Tao Ma[3], Stephany Y. Tzeng[5], Yassine Daoud[1], Jordan J. Green[1,5], Gregg L. Semenza[6], Silvia Montaner[3]*, and Akrit Sodhi[1]*

[1]Wilmer Eye Institute, Johns Hopkins University School of Medicine, Baltimore, MD 21287, USA
[2]Department of Ophthalmology, the Fourth Affiliated Hospital of China Medical University, Eye Hospital of China Medical University, Key Lens Research Laboratory of Liaoning Province, China
[3]Department of Oncology and Diagnostic Sciences, School of Dentistry, Greenebaum Cancer Center, University of Maryland, Baltimore, MD 21201, USA
[4]State Key Laboratory of Ophthalmology, Clinical Research Center, Zhongshan Ophthalmic Center, Sun Yat-Sen University, Guangzhou, China
[5]Department of Biomedical Engineering, Institute for NanoBioTechnology, and the Translational Tissue Engineering Center, Johns Hopkins University School of Medicine, Baltimore, MD, 21231, USA
[6]Departments of Genetic Medicine, Pediatrics, Medicine, Oncology, Radiation Oncology, and Biological Chemistry, Johns Hopkins University School of Medicine, Baltimore, MD, 21205, USA

*Correspondence:

Akrit Sodhi, M.D., Ph.D.
Wilmer Eye Institute, Johns Hopkins School of Medicine
400 N. Broadway St., Smith Building, 4039
Baltimore, MD 21287, United States
FAX: 410-614-8577
Email: asodhi1@jhmi.edu

Silvia Montaner, Ph.D, M.P.H.
Department of Oncology and Diagnostic Sciences
University of Maryland, Baltimore
650 W. Baltimore Street, 7th North, Rm 7263
Baltimore, MD 21201, United States
FAX: (410) 706-6115
E-mail: smontaner@umaryland.edu

Conflict of Interest: A.S. and G.L.S. are the co-founders of and hold equity in HIF Therapeutics, Inc. A.S. is a member of the Board of Directors and serves as the CEO. G.L.S. is also a member of the Board of Directors and serves as the President. This arrangement has been reviewed and approved by the Johns Hopkins University in accordance with its conflict of interest policies. J.G. is an inventor on patent applications related to this work filed by Johns Hopkins University (PCT/US2019/055741 Filed October 10, 2019, 17/282,939 Filed April 5, 2021).

Funding: This work was supported by the National Eye Institute, National Institutes of Health grants R01EY029750 to A.S., R01EY025705 to S.M. and A.S, R01EY031097 to J.J.G., and EY001765 (the Wilmer Core Grant for Vision Research, Microscopy and Imaging Core Module); the Research to Prevent Blindness, Inc., Special Scholar Award to A.S., Sybil B. Harrington Stein Innovation Award to G.L.S., and an unrestricted grant to the Wilmer Eye Institute; the Alcon Research Institute to A.S.; and the Branna and Irving Sisenwein Professorship in Ophthalmology to A.S.. The funding organizations had no role in the design or conduct of this research.

Authors' Contributions: A.S. and S.M. are the primary contributors to research design. Y.Q., A.D., K.J, M.R., X.C., J.C.S., C.G., J.Z., J.V., D.M., N-S.K., T.M., S.T., and Y.D. are responsible for research execution and are contributors to data acquisition. A.S., Y.Q., A.D., K.J., M.R., X.C., J.C.S., C.G., J.Z., D.M, T.M., S.T., J.J.G., and S.M. are the primary contributors to data analysis and interpretation. Manuscript preparation by A.S. and S.M., with revisions provided by Y.Q. and G.L.S..

Running head: ANGPTL4 Contribution to CNV in wet AMD

Key Words: Vascular endothelial growth factor (VEGF), Angiopoietin-like 4 (ANGPTL4), Hypoxia Inducible Factor (HIF), neovascular age-related macular degeneration (nvAMD), choroidal neovascularization (CNV), angiogenesis, anti-VEGF therapy, aqueous fluid, biomarker

Abstract

Most patients with neovascular age-related macular degeneration (nvAMD), the leading cause of severe vision loss in elderly Americans, respond inadequately to current therapies targeting a single angiogenic mediator, vascular endothelial growth factor (VEGF). Here we report that aqueous levels of a second vasoactive mediator, angiopoietin-like 4 (ANGPTL4), can help predict the response of nvAMD patients to anti-VEGF therapies. ANGPTL4 expression was higher in patients who required monthly treatment with anti-VEGF therapies compared to patients who could be effectively treated with less frequent injections. We further demonstrate that ANGPTL4 acts synergistically with VEGF to promote the growth and leakage of choroidal neovascular (CNV) lesions in mice. Targeting ANGPTL4 expression was as effective as targeting VEGF expression for treating CNV in mice, while simultaneously targeting both was more effective than targeting either factor alone. To help translate these findings to patients, we used a soluble receptor that binds to both VEGF and ANGPTL4 and effectively inhibited the development of CNV lesions in mice. Our findings provide an assay that can help predict the response of nvAMD patients to anti-VEGF monotherapy and suggest that therapies targeting both ANGPTL4 and VEGF will be a more effective approach for the treatment of this blinding disease.

Introduction

Neovascular or "wet" age-related macular degeneration (nvAMD) is a leading cause of severe vision loss in elderly Americans (1). The growth of abnormal leaky blood vessels (i.e., choroidal neovascularization or CNV) in these patients can lead to rapid and often irreversible vision loss (2). The recent introduction of therapies targeting vascular endothelial growth factor (VEGF), a potent endothelial mitogen and permeability factor, has had a remarkable impact on patients with nvAMD who previously suffered vision loss from edema, bleeding and scarring caused by CNV (3). However, anti-VEGF therapies are administered chronically every 1-2 months, raising concerns about the substantial economic and social burden of frequent clinic visits for elderly patients who often require assistance for transportation and mobility (4). This is particularly relevant given emerging ethical issues about the distribution of "cost-effective" vs. "most effective" anti-VEGF therapies among patients with ocular neovascular disease (5). There are also concerns about ocular risks – and concerns based on preclinical data about the safety – of frequent, chronic intraocular injections of anti-VEGF therapies (6, 7). This has prompted investigators to explore alternative approaches that refine initial treatment protocols without sacrificing the visual acuity benefits observed with monthly or bi-monthly treatment.

In this regard, we recently described a hybrid of the treat-and-extend (TAE) and *pro re nata* (PRN) protocols, which we designated treat-and-extend, pause and monitor (TEP/M) in which patients initially undergo 3 consecutive monthly injections with anti-VEGF therapy, followed by a TAE protocol in which the interval for the next treatment is extended (by two weeks) for patients who demonstrate an absence of activity (8). Patients who remain quiescent 12 weeks from their prior treatment enter a "treatment pause" and are switched to PRN treatment; treatment is resumed based on a decline in vision or worsening on clinical exam

and/or imaging studies. Using this approach, we reported that patients with nvAMD at the end of one year can be divided into three groups: a) patients who require monthly treatment with anti-VEGF therapy (i.e., patients who fail treatment extension; ~20% of patients); b) patients who require less frequent but ongoing treatment with anti-VEGF therapy (~50% of patients); and c) patients who can be successfully weaned off treatment with anti-VEGF therapy (~30% of patients) (8). Interestingly, neither the pre- nor post-treatment aqueous levels of VEGF correlated with the need for more – or less – frequent treatment with anti-VEGF therapy (8), suggesting that other vasoactive mediators may contribute to the response of nvAMD patients to treatment.

Collectively, these observations emphasize the importance of ongoing efforts to identify other factors that contribute to the development of CNV and that may therefore serve as molecular biomarkers and/or influence the response of nvAMD patients to anti-VEGF therapies. Of interest, the transcriptional activator hypoxia-inducible factor (HIF)-1 has been hypothesized to play a critical role in regulating the pathologic expression of numerous angiogenic mediators (including VEGF) that together promote ocular neovascularization (9, 10). In nvAMD, it is hypothesized that outer retinal ischemia due to interruption of oxygen delivery from the choriocapillaris to the overlying RPE results in HIF-1α accumulation (11). Indeed, it has been reported that the choriocapillaris underlying the macula becomes attenuated (and its function compromised) with aging (12). In patients with AMD, material (i.e., drusen) accumulates underneath and within the thickened RPE basement (Bruch's) membrane, forming a physical barrier for O_2 diffusion and further exacerbating the reduced oxygen delivery to the overlying RPE (13). This, in turn, is thought to result in the pathological accumulation of HIF-1α in the RPE of nvAMD patients.

There is considerable pre-clinical evidence that HIF-1 participates in the regulation of VEGF expression and the development of CNV in patients with wet AMD (14). Increased expression of HIF-1α has been reported in CNV membranes in AMD eyes (15, 16). Inhibition of HIF-1 in the RPE, using either pharmacologic (17) or RNA interference (18) strategies, decreases the size of CNV lesions in mouse models. We therefore set out to examine the contribution of HIF-regulated angiogenic factors, in addition to VEGF, in the promotion of CNV.

Results

Increased ANGPTL4 expression in nvAMD patients who respond inadequately to anti-VEGF therapy.

To identify vasoactive factors that could influence the response of these nvAMD patients to anti-VEGF therapy, we shifted our attention upstream from VEGF to the transcription factor that regulates its expression, HIF-1, the master regulator of genes encoding angiogenic mediators (19). Evidence has converged on one HIF-regulated vasoactive mediator, angiopoietin 2 (ANGPT2), in ocular neovascular disease, and specifically in the development of CNV in patients with nvAMD (20). ANGPT2 acts synergistically with VEGF to promote angiogenesis but is anti-angiogenic in the absence of VEGF (21). It has previously been reported that ANGPT2 promotes the development of vascular permeability and pathological angiogenesis in animal models of nvAMD (22, 23). Expression of ANGPT2 mRNA (24) and protein (25) has been detected in surgically excised CNV membranes from patients with nvAMD. This led to speculation that ANGPT2 expression may contribute to the modest response of some nvAMD patients to anti-VEGF therapy (26, 27). Consequently, there are ongoing and recently completed clinical trials examining the safety and efficacy of therapies directly or indirectly targeting ANGPT2 and its downstream receptor, TIE2, in patients with nvAMD (28, 29). To determine if ANGPT2 expression influenced the response of nvAMD patients to anti-VEGF therapy, we examined levels of ANGPT2 in patients treated with anti-VEGF therapy using the TEP/M protocol. We did not observe a difference in the aqueous levels of ANGPT2 in patients who required monthly treatment with anti-VEGF therapy compared to patients who required less frequent treatment, or those who could be weaned off treatment (Fig. 1A; Supplemental Table 1). We also did not observe differences in the aqueous levels of another HIF-regulated vasoactive

mediator which had also been previously implicated in the pathogenesis of nvAMD, erythropoietin (EPO) (30, 31), in patients who responded inadequately to anti-VEGF therapy (Fig. 1B). While these data do not rule out a role for therapies targeting ANGPT2 or EPO for the treatment of CNV, they suggest that additional vasoactive mediators may contribute to the inadequate response of some nvAMD patients to current anti-VEGF therapies.

Another HIF-regulated angiogenic mediator, angiopoietin-like 4 (ANGPTL4) has been implicated in pathological angiogenesis in ischemic retinal disease (32-34). We observed an increase in the levels of ANGPTL4 in the aqueous of patients who required injections every 4 weeks (i.e., patients who failed treatment extension) using the TEP/M protocol compared to non-AMD controls (Fig. 1C). However, increased aqueous ANGPTL4 levels were not detected in patients who could be extended to 6-8 weeks or 10-12 weeks, or who entered a treatment pause by the end of 1 year (Fig. 1C). Moreover, the aqueous levels of ANGPTL4 were lower in patients who could be extended to every 10-12 weeks or patients who entered a treatment pause by the end of 1 year compared to patients who required every 4-week injections (Fig. 1C). Collectively, these data suggest that aqueous levels of ANGPTL4 may help predict the response of nvAMD patients to anti-VEGF therapy.

ANGPTL4 is a biomarker for the response of nvAMD patients to anti-VEGF therapy.

We next generated a receiving operating characteristics (ROC) curve to determine whether aqueous levels of ANGPTL4 could be an effective biomarker for patients who require monthly treatment with anti-VEGF therapy. To this end, an ROC for aqueous ANGPTL4 was generated and at a cut off of 4.22 ng/mL the sensitivity for predicting which patients would require monthly injection was 91% with a specificity of 68% (Fig. 2A). Although the sample size

is small, this suggests that ANGPTL4 may be an effective biomarker for predicting the response of nvAMD patients to treatment with anti-VEGF therapy. ROC curves for VEGF (with a cut off of 260 pg/mL) and ANGPT2 (with a cut off of 1.10 ng/mL) had lower sensitivity (83% and 71 %, respectively) and specificity (53% and 45%, respectively) compared to ANGPTL4 (Figs. 2B and C). However, by combining the results for VEGF and ANGPTL4, the sensitivity for predicting which patients would require monthly injection was 76% with a specificity of 85% (Supplemental Table 2). These results suggest that pre-treatment levels of VEGF and early levels of ANGPTL4 could help predict how patients with nvAMD will respond to treatment with anti-VEGF therapy.

Increased ANGPTL4 expression in the aqueous of nvAMD patients with active CNV.

To further characterize the expression of ANGPTL4 in nvAMD patients being treated in the clinic for active CNV, we obtained aqueous samples from untreated, newly diagnosed nvAMD patients (nvAMD UnTx) who were initiating treatment with anti-VEGF therapy and examined the levels of ANGPTL4 compared to aqueous samples obtained prior to the initiation of cataract surgery from patients without AMD (Control) and patients with non-neovascular or "dry" AMD (nnvAMD) (Supplemental Table 3). The mean levels of VEGF and ANGPTL4 were not significantly different between control patients without AMD and patients with nnvAMD (Fig. 3A and B). However, we observed significantly increased expression of both VEGF (1.5-fold; $P<0.0001$) and ANGPTL4 (2.7-fold; $P<0.0001$) in the aqueous of treatment-naïve (i.e. no history of anti-VEGF therapy) nvAMD eyes compared to control eyes, as well as compared to nnvAMD eyes (1.5-fold and 2.4-fold, respectively; both $P<0.01$).

We next examined whether ANGPTL4 levels were also increased in aqueous fluid from

patients who had a history of anti-VEGF therapy, but had not been treated in ≥ 12 weeks prior to sample collection, and who had evidence of active ("recurrent") CNV (nvAMD Recurrent; Supplemental Table 3). We observed increased mean VEGF (1.5-fold; $P<0.0001$) and ANGPTL4 (4.6-fold; $P<0.0001$) levels in the aqueous of nvAMD Recurrent patients compared to control eyes, as well as compared to eyes of patients with nnvAMD (1.4-fold and 4.1-fold, respectively; $P<0.0001$ and $P<0.01$, respectively) (Fig. 3A and B; Supplemental Fig. 1). Collectively, these results suggest that ANGPTL4 may be a therapeutic target for patients with newly diagnosed and recurrent CNV.

For therapies targeting ANGPTL4 to be effective in patients already receiving currently available therapies targeting VEGF, ANGPTL4 levels would need to remain increased despite receiving anti-VEGF treatments. To assess the levels of ANGPTL4 after initiation of intravitreal anti-VEGF therapy, aqueous samples from patients were obtained 4 to 6 weeks after their first treatment with anti-VEGF therapy and were analyzed (nvAMD 1st Tx; Supplemental Table 3). Mean ANGPTL4 levels in this group remained increased compared to control and nnvAMD eyes (3.4-fold and 3-fold, respectively; $P<0.0001$ and $P<0.01$, respectively; Fig. 3C). Collectively, these studies indicate that ANGPTL4 expression is increased in nvAMD patients with active CNV, including patients who have either a recent or remote history of anti-VEGF therapy.

ANGPTL4 expression in CNV lesions in nvAMD eyes.

To confirm that ANGPTL4 expression was increased within CNV lesions in patients with nvAMD, we examined autopsy eyes from patients with a known diagnosis of nvAMD with active CNV by histopathology (Fig. 4A and B); adjacent tissue without evidence of CNV was used as a control. Expression of VEGF by the RPE has been reported to be important for

maintaining the health of the choriocapillaris (12, 35, 36). Accordingly, immunohistochemical analysis of CNV lesions demonstrated light staining for VEGF in the RPE and choroid without active CNV (Fig. 4C). Strong staining for VEGF was detected within CNV lesions (Fig. 4C), as has previously been described (36). We observed a similar pattern for ANGPTL4 expression, with light staining within the choroid without active CNV, but strong staining for ANGPTL4 within CNV lesions in 4 out of 4 nvAMD eyes examined (Fig. 4D). IgG was used as a negative control (Fig. 4E). Collectively, these data demonstrate that expression of ANGPTL4, similar to VEGF, is observed in the choriocapillaris and within CNV lesions in the eyes of nvAMD patients.

HIF-1-dependent ANGPTL4 expression in the laser-induced CNV model of nvAMD.

To examine further whether ANGPTL4 directly contributes to the development of CNV in patients with nvAMD, we employed a mouse model of CNV, in which a laser is used to rupture Bruch's membrane (37). The laser CNV model has proven to be a powerful tool to examine molecular events underlying the development of CNV (38). We observed increased expression of *Angptl4* mRNA over time in the RPE/choroid of lasered eyes compared to non-lasered contralateral (control) eyes (Fig. 5A). Examination of laser CNV lesions by immunofluorescence demonstrated ANGPTL4 expression within CNV lesions, extending from the RPE to the overlying CNV tissue (Fig. 5B), similar to what was observed in CNV lesions from patients with nvAMD (Fig. 4D).

We next set out to determine whether HIF-1α expression influenced ANGPTL4 expression in CNV lesions. To this end, we used mice that were heterozygous for a knockout allele at the *Hif1a* locus (*Hif1a*$^{+/-}$) (39). Basal levels of HIF-1α are relatively normal in *Hif1a*$^{+/-}$

mice, whereas in response to ischemia, HIF-1α expression is largely unchanged in *Hif1a*$^{+/-}$ mice but potently stimulated in wild type (wt) littermate controls (40). CNV lesions in *Hif1a*$^{+/-}$ mice were small compared to wt littermate controls (Fig. 5C). This corresponded to a marked decrease in *Vegf* and *Angptl4* mRNA expression (Fig. 5D and E).

Synergism between VEGF and ANGPTL4 in the pathogenesis of CNV.

It has previously been reported that ANGPTL4, along with VEGF, stimulates vascular permeability (34, 41) and pathological angiogenesis (32, 42) in pre-clinical models of ischemic retinal disease. We hypothesized that CNV lesions may similarly be dependent on both VEGF and ANGPTL4 expression. To test this hypothesis, we first analyzed the effect of ANGPTL4 on tubule formation (an in vitro proxy for angiogenesis) in an immortalized mouse retinal endothelial cell (iREC) line (43) in the absence or presence of VEGF. Recombinant mouse (rm) ANGPTL4 induced iREC tubule formation (increasing tube length and number of nodes; Fig. 6A and B), similar to rmVEGF. Interestingly, treatment of iRECs with both factors resulted in a greater effect than either factor alone (Fig. 6A and B).

To examine in vivo the contribution of ANGPTL4 to the development of CNV, we took advantage of a transgenic model of CNV. In the laser CNV model, increased *Vegf* mRNA expression is observed in the region of laser injury (Fig. 6C). The increased expression of *Vegf* mRNA in the outer retina of mice is reproduced in the *rho*-h*VEGF* transgenic mouse (Fig. 6D), in which the human VEGF is constitutively expressed under the rod-specific rhodopsin promoter (44). The *rho*-h*VEGF* transgenic mouse has previously been reported to reproduce CNV-like lesions that are observed as early as 3 weeks of age (44). To investigate the ability of ANGPTL4 to modulate VEGF-induced CNV, we administered subretinal injections of rmANGPTL4 in 2-

week old *rho*-h*VEGF* mice (Fig. 6E). Although the modest increase in CNV lesion number 72 hours after subretinal injection of rmANGPTL4 compared to PBS control was not significant, we observed a marked increase in CNV lesions size and leakage, as assessed by fluorescein angiography (FA) (Fig. 6F). The increase in CNV lesions size after subretinal injection of rmANGPTL4 was corroborated using fluorescein-conjugated isolectin B4 to stain CNV lesions on choroidal flat mounts 72 hours following injection compared to PBS control (Fig. 6G). Collectively, these results suggest that ANGPTL4 enhances the size of – and leakage from – CNV lesions induced by forced expression of VEGF in mice.

Targeting ANGPTL4, VEGF, or both for treating CNV in mice.

To examine whether ANGPTL4 may be required for the development of CNV, we took advantage of a novel RNAi approach to knock down expression of genes in the mouse eye (45). We generated siRNA-encapsulating nanoparticles using reducible branched ester amine quadpolymers (rBEAQs; Fig. 7A; Supplemental Fig. 2) (46). These biodegradable nanoparticles are designed to escape the endosomal compartment and then release siRNA cargo in an environmentally triggered manner upon cleavage of disulfide bonds in the polymer backbone in the reducing cytosolic environment. Intraocular injection with the nanoparticle complexed with scrambled siRNA (NP-scr) conjugated to a fluorophore (Cy5) demonstrated effective transfection of retinal cells in the outer retina, as well as the underlying RPE 24 hours after a single intravitreal injection (Fig. 7B).

We used these biodegradable polymeric nanoparticles to deliver HIF-1α siRNA (NP-HIF) and observed robust knockdown of HIF-1α protein in hypoxic primary mouse RPE cells (Fig. 7C), similar to transfection utilizing a lipid-based commercial reagent encapsulating HIF-

1α siRNA (Lipo-HIF). Accordingly, we observed potent knockdown of *Hif1a* mRNA expression in vivo at 5 days after intraocular administration of NP-HIF (Fig. 7D), resulting in a reduction in *Vegf* and *Angptl4* mRNA expression compared to scrambled siRNA (NP-scr) control (Fig. 7E). To assess the effect of NP-HIF on CNV lesions, we treated mice with a single intraocular injection of NP-HIF or NP-scr at day 1 (Fig. 7F). NP-HIF potently inhibited the development of CNV in response to laser injury (Fig. 7G), similar to what was observed with in *Hif1a*$^{+/-}$ mice Fig. 5C).

To evaluate the contribution of ANGPTL4 to the development of CNV in mice, we next encapsulated *Angptl4* siRNA (NP-ANPGLT4); *Vegf* siRNA (NP-VEGF) was used as a control. Intravitreal injection with NP-VEGF or NP-ANGPTL4 resulted in knockdown of *Vegf* (Fig. 7H) or *Angptl4* (Fig. 7I) mRNA expression, respectively. Treatment of laser CNV mice with a single intraocular injection of NP-ANGPTL4 1 day after laser injury resulted in decreased area of CNV lesions on day 7 compared to NP-scr control (Fig. 7J). There was no difference in CNV lesion area in animals treated with NP-VEGF compared to NP-ANGPTL4 (Fig. 7J), indicating that therapies targeting ANGPTL4 are as effective as therapies targeting VEGF in this model. To evaluate the therapeutic potential of combining anti-VEGF and anti-ANGPTL4 therapies, we performed intravitreal injections of both NP-VEGF and NP-ANGPTL4 together. This resulted in a further decrease CNV lesion area compared to injection with either NP-VEGF or NP-ANGPLT4 alone (Fig. 7J). Collectively, these results suggest that therapies targeting ANGPTL4 could be effective alone, but would also enhance the efficacy of current anti-VEGF therapies for the treatment of patients with nvAMD.

Targeting both VEGF and ANGPTL4 with a soluble receptor, sNRP1, effectively inhibits

CNV in mice.

We recently demonstrated that the endothelial cell receptor, neuropilin (NRP), binds to ANGPTL4 to promote Rho activation and increase vascular permeability (41) (Fig. 8A). We therefore knocked down NRP1 and NRP2 expression with RNAi in human umbilical vein endothelial cells (HUVECs) to examine the role of this receptor on the promotion of pathological angiogenesis mediated by ANGPTL4 (Fig. 8B). We observed impaired rhANGPTL4-mediated endothelial cell tubule formation following knock down of NRP1 or NRP2 (Fig. 8C), indicating that NRPs are also required for pathological angiogenesis mediated by ANGPTL4.

Soluble NRPs (sNRPs) are naturally occurring fragments of NRPs that lack the transmembrane and intracellular domains (Fig. 8D). They are expressed independent from intact NRPs and function as endogenous inhibitors of the biological effects of NRP signaling by acting as traps for the NRP ligands (47). sNRP1 has previously been reported to inhibit the binding of VEGF to full-length NRP1 and both sNRP1 and sNRP2 have been shown to inhibit tumor angiogenesis and growth (48, 49). We recently reported that sNRP1 also prevents binding of ANGPTL4 to NRP1 and NRP2 and inhibits vascular permeability mediated by ANGPTL4 (41). Treatment of iRECs with recombinant human sNRP1 resulted in a potent inhibition of ANGPTL4-induced iREC tubule formation, similar to what was observed for VEGF-mediated tubule formation (Fig. 8E). These results suggested that sNRP could provide an effective approach to block the effects of both ANGPTL4 and VEGF.

As sNRP1 is an endogenous inhibitor of ANGPTL4 and VEGF, we next examined whether its expression was influenced by the presence of CNV in the eyes of patients with nvAMD. While expression of sNRP1 was detected in the eyes of patients with nvAMD, it was not increased compared to control patients without AMD (Fig. 8F). Collectively, these

observations exposed a potential therapeutic approach for the inhibition of CNV in patients with nvAMD using exogenous sNRP1. We therefore examined the effect of treating CNV in mice with recombinant human (rh)sNRP1. A single intraocular injection of rhsNRP1 was able to inhibit CNV compared to control mice that were treated with vehicle (PBS) (Fig. 8G). Collectively, these studies demonstrate that VEGF and ANGPTL4 contribute synergistically to the promotion of CNV lesions in nvAMD patients (Fig. 9) and suggest that therapies targeting both ANGPTL4 and VEGF will be the most effective therapeutic approach for the treatment of nvAMD.

Discussion

Despite affecting only 10% of patients with AMD, CNV is the cause of severe vision loss in 90% of AMD patients (50). Over the last 20 years, a large body of data has demonstrated that VEGF plays a fundamental role in the pathogenesis of CNV in patients with nvAMD (51). This finding led to the development of therapies that specifically target VEGF and ushered in a new era in the treatment of this vision-threatening disease (50). Anti-VEGF therapies have had a remarkable impact on nvAMD patients who previously suffered major vision loss from edema, bleeding or scarring caused by CNV (3). Nonetheless, less than half of nvAMD patients treated with anti-VEGF therapies have a major improvement in visual acuity (i.e., a gain of at least 15 letters – or 3 lines – on the ETDRS visual acuity chart) despite monthly or bimonthly injections. Moreover, the majority of patients who do respond to anti-VEGF therapy still have intraretinal or subretinal fluid (50). These studies suggest that additional vasoactive factors contribute to CNV pathogenesis and vision loss in nvAMD patients.

In this regard, studies using animal models have demonstrated that expression of a constitutively-active form of the transcription factor HIF-1α was sufficient to promote ocular neovascularization in vivo (52) while expression of VEGF alone was not sufficient to mediate this effect (53-55). These results implicate additional HIF-regulated angiogenic factor(s) in the promotion of pathological neovascularization in the eye. Here we examine the contribution of HIF-regulated angiogenic factors, in addition to VEGF, in the promotion of CNV.

Using a hybrid of TAE and PRN protocols, which we designated treat-and-extend, pause and monitor (TEP/M), we recently reported that ~30% of patients with nvAMD can be safely weaned off anti-VEGF therapy within 1 year (8). However, ~20% of nvAMD patients failed treatment extension, requiring intraocular injections with anti-VEGF therapy every four weeks.

Most of these patients still had fluid despite this aggressive treatment regimen (8). These results demonstrate that a subset of nvAMD patients are less sensitive to currently available anti-VEGF therapies, and implicate other vasoactive mediators in the promotion of CNV in these patients. We demonstrate here that aqueous levels of ANGPT2, a key target for emerging therapies for nvAMD (26-29, 56-58), were unchanged in patients who responded well – or poorly – to anti-VEGF therapy. Conversely, aqueous levels of another HIF-regulated vasoactive factor, ANGPTL4, correlated inversely with patients' response to anti-VEGF therapy. Levels of ANGPTL4 in the aqueous of nvAMD patients who required q4 week injections were higher than nvAMD patients who required q10-12 week injections or those patients who entered a treatment pause. These data suggest that patients with higher aqueous levels of ANGPTL4 may be better suited for longer-acting anti-VEGF agents. Conversely, patients with low levels of ANGPTL4 may be adequately treated with currently available anti-VEGF therapies. Additional studies will be needed to determine if aqueous levels of ANGPTL4 (and VEGF) at the time of treatment initiation could be used as biomarkers to help predict which patients would benefit from long-acting anti-VEGF therapies.

In addition to its role as a potential biomarker, we further observed that ANGPTL4 contributes to the size of, and leakage from, CNV lesions induced by VEGF over-expression in mice, supporting a synergistic role for ANGPTL4 – in combination with VEGF – in the promotion of CNV (Fig. 9). We have previously demonstrated that ANGPTL4 can promote both angiogenesis (32, 42) and vascular permeability (34, 41, 59), the latter through promotion of the Rho/ROCK pathway (41). In addition to regulating angiogiogenesis, ANGPTL4 has also been reported to regulate lipid metabolism (60) and inflammation (61), both of which have also been implicated in the pathogenesis of AMD (62, 63). Additional studies will be necessary to

determine the mechanism(s) by which ANGPTL4 contributes to the development of CNV in patients with nvAMD.

Although we did not observe a correlation between the size of CNV lesions in AMD patients and the aqueous levels of ANGPTL4, as has previously been reported (64), levels of ANGPTL4 remained increased in the aqueous of nvAMD patients being treated for active CNV compared to control patients without AMD, or patients with nnvAMD. Increased ANGPTL4 levels were observed in patients with a recent (within 4-6 week) or remote (>12 weeks) history of anti-VEGF therapy, suggesting that elevated ANGPTL4 levels were not dependent on elevated VEGF levels, and that therapies targeting ANGPTL4 could be used in conjunction with current therapies targeting VEGF. Persistent expression of ANGPTL4 in the eyes of nvAMD patients may help explain why the majority of patients receiving monthly injections with anti-VEGF therapy have intraretinal and/or subretinal fluid despite treatment (50). The increased expression of ANGPTL4 in nvAMD compared to nnvAMD patients may further help explain why prophylactic treatment of patients with nnvAMD with anti-VEGF therapy failed to prevent their conversion to nvAMD (65).

Using an in vivo biodegradable nanoparticle-encapsulated siRNA approach, we demonstrate that targeting either ANGPTL4 or VEGF was equally effective in preventing the development of CNV lesions in mice. This suggests that therapies targeting ANGPTL4 may be an alternative approach for the treatment of nvAMD. We further observe that combining therapies targeting both VEGF and ANGPTL4 was more effective for the treatment of CNV in mice than targeting either vasoactive mediator alone. These observations suggest that therapies targeting both ANGPTL4 and VEGF may be a more effective approach for the treatment of CNV.

In this regard, we have recently reported that the endothelial cell receptors NRP1 and NRP2 are essential for the promotion of vascular hyperpermeability by ANGPTL4, similar to VEGF (41). We further observed that ANGPTL4 binds both NRP1 and NRP2 with comparable affinities to VEGFA/NRPs binding. Using a soluble receptor for neuropilin (sNRP1) that targets both VEGF and ANGPTL4 (41), we were able to effectively inhibit the promotion of endothelial cell tubule formation by ANGPTL4 and VEGF in vitro and CNV lesions in mice.

In addition to ANGPTL4 and VEGFs, NRP receptors have also been reported to bind to other vasoactive mediators, including Semaphorin3s, fibroblast growth factor, platelet-derived growth factor, hepatocyte growth factor, and transforming growth factor-beta 1 (47, 66). sNRPs may therefore affect CNV lesions by inhibiting a broad spectrum of vasoactive mediators. While expression of sNRP1 was observed in the eyes of patients with nvAMD, there were not elevated compared to controls. Collectively, these studies provide a foundation for the early clinical assessment of intraocular injections with sNRPs – alone or in combination with current anti-VEGF therapies – in the treatment of patients with nvAMD.

Materials and Methods

Cells culture and Reagents

Immortal mouse retinal endothelial cells (iREC) isolated from immortomice were a generous gift from Dr. Jeremy Nathans (Johns Hopkins University School of Medicine, Baltimore, Maryland) and were cultured as previously described (43). Human umbilical vein endothelial cells (HUVECs) were cultured as previously described (67). All cell lines were routinely tested for Mycoplasma contamination by PCR.

To isolate the primary RPE cells from mice, the eyes from postnatal day (P)1-P5 mice were enucleated and digested in 0.2% dispase for 30 minutes on shaker and then washed in DMEM containing 4.5 g/l of glucose for 3 times. The eyes were then dissected to separate the neurosensory retina from the underlying RPE/choroid; the latter was then washed with PBS and then digested in 0.5% trypsin for 45 minutes. The lysate was then washed in DMEM containing 4.5 g/l of glucose and then centrifuged. The supernatant was removed and DMEM containing 4.5 g/l of glucose was used to resuspend the lysate and then pipetted up and down to physically digest the RPE cells. The lysate was then plated in DMEM containing 4.5 g/l of glucose with 10% FBS.

Alflibercept (Eylea^{TM}) was purchased from the Johns Hopkins Pharmacy. Recombinant human or murine ANGPTL4 (rhANGPTL4, rmANGPTL4), and human or murine VEGFA (rhVEGF, rmVEGF) were purchased from R&D Systems. Recombinant human sNRP1 was purchased from ReliaTech.

Quantitative Real-Time PCR (RT-qPCR)

Primers are listed in Supplemental Table 4.

Total RNA was isolated from culture cells or retinas with PureLink™ RNA Mini Kit (Invitrogen #12183025), and cDNA was prepared with MuLV Reverse Transcriptase (Applied Biosystems). Quantitative real-time PCR was performed with Power SYBR Green PCR Master Mix (Applied Biosystems) and MyiQ Real-Time PCR Detection System (Bio-Rad). Normalization was done using Peptidylprolyl Isomerase A (PPIA) for mouse tissue and cell lines.

Western Blot

Antibodies are listed in Supplemental Table 5.

Cells and RPE/choroid lysates were lysed using radioimmunoprecipitation assay (RIPA) buffer (Sigma-Aldrich Corp., St. Louis, MO, USA) with 10% protease inhibitor cocktail (Cell Signaling, Danvers, MA, USA). Cell lysates were then solubilized in lithium dodecyl sulfate (LDS)-sample buffer (Life Technologies, Carlsbad, CA, USA) and incubated for 5 minutes at 95°C. Lysates were subjected to 4% to 12% gradient SDS/PAGE (Life Technologies). After blocking with 5% milk (Bio-Rad, Hercules, CA, USA), the membrane was incubated with primary antibody overnight at 4°C. After washing, the membrane was incubated with (HRP)-conjugated anti-mouse or anti-rabbit IgG (Cell Signaling) for 1 hour and then visualized with ECL SuperSignal West Femto (Thermo Scientific, Rockford, IL, USA). Western blot scans are representative of at least three independent experiments.

In vitro Tube Formation Assay

iRECs (8000 cells/well) were plated on 10μL of Matrigel basement membrane matrix - growth factor reduced (Corning, #35623) on μ-Angiogenesis slides (Ibidi, #81506) in presence of the angiogenic factors in 1% serum containing DMEM. The tubes that formed were imaged 16

hours post-plating on Cytation 5 imaging multimode reader (Biotek Instruments). Phase contrast images were analyzed for tube length using Angiogenesis Analyzer plugin on Image J (Version 1.52a).

Mice

Eight-week-old pathogen-free female C57BL/6 mice were obtained from Jackson Laboratory. *Hif1a*$^{+/-}$ have been previously described (39). *rho*-h*VEGF* mice (44) were obtained from Dr. Peter Campochiaro (Johns Hopkins School of Medicine, Baltimore, MD).

siRNA

Hif1a siRNA*, ANGPTL4* siRNA*, Vegf* siRNA and a nontargeting control siRNA were purchased from Ambion. Predesigned control (scrambled or scr), NRP1, NRP2 siRNA sequences were obtained from Qiagen. siRNA delivery to cells was performed using Hiperfect (Qiagen).

Intraocular Injections

Intravitreal and subretinal injections were performed with a (PLI-100A) Pico-liter Microinjector (Warner Instruments, Harvard Bioscience) using pulled-glass micropipettes. Each micropipette was calibrated to deliver a 1-μL volume on depression of a foot switch. The mice were anesthetized with ketamine (100 mg/kg) and xylazine (5mg/kg) mixture and under a dissecting microscope after pupils were dilated with tropicamide (Alcon Laboratories). The sharpened tip of the micropipette was passed through the sclera just posterior to the limbus into the vitreous cavity and visualized through the dilated pupil. For intravitreal injections, the foot

switch was depressed, which caused fluid to penetrate into the vitreous space. For subretinal injections, the tip of the micropipette was advanced to the surface of the neurosensory retina and the foot switch was depressed, which caused fluid jet to penetrate through the neurosensory retina into the subretinal space.

Fluorescein Angiography (FA)

72 hours after administration of PBS or recombinant murine (rm)ANGPTL4 subretinal injections, two-week-old *rho*-h*VEGF* mice were anesthetized by ketamine (100mg/kg) and xylazine (5 mg/kg) mixture and pupils were dilated with tropicamide (Alcon laboratories) and lubricated with hypromellose eye drops (Alcon Laboratories). 5ul of 10% Sterile Fluorescein Sodium solution (AK-FLUOR@10%) was injected intraperitoneally after the mice were anesthetized. The color fundus photographs and fundus fluorescein angiograms were taken in micron III of Wilmer core facility.

The FA images were taken in various positions such as central, superior, inferior, temporal, nasal and the lesion numbers were counted manually. The pixel size of lesions was converted to mm^2 by using the following formula. The lesion size (mm^2) = (fundus area (7.07))/(fundus pixel size (480000)) x pixel size of the lesion. The quantification area of lesions and fluorescence intensity were done by Image J software.

Laser CNV Model

Laser CNV model in which laser is used to rupture Bruch's membrane in mice was performed as previously described (68). Briefly, 10-12 week-old mice were anesthetized with a mixture of ketamine (100 mg/kg) and xylazine (5 mg/kg) after pupils were dilated with

tropicamide (Alcon Laboratories). Lubricating hypromellose eye drops (Alcon Laboratories) were applied to the cornea. The fundus was viewed using a hand-held coverslip as a contact lens and laser photocoagulation was performed using the diode laser photocoagulator (IRIS Medical, Mountain View, CA) and the slit lamp delivery system. Three to four laser burn spots equidistant from the optic nerve using a wavelength of 532 nm, a power of 160-190 milliwatt, a duration of 100 ms, and a spot size of 75 μm were performed for each eye. Treatments (when indicated) provided on day 3, including aflibercept (800 ng, PBS with equal volume as vehicle control) or nanoparticle (NP)-RNA interference (RNAi) were introduced by intravitreal injection as described above. Animals were sacrificed at day 7, eyes were enucleated and further studies conducted for immunofluorescence of laser CNV lesions (described below).

In situ hybridization

RNA in situ hybridization was performed with RNAscope® 2.5 HD Duplex Detection Reagent Kit (ACD, #323350) following the manufacturer's protocol. Fresh eyecups, without prior fixation, were embedded into OCT compound (Tissue-Tek) and immediately frozen by liquid nitrogen. The frozen blocks were sectioned at a thickness of 14 μm and were assayed for mouse *Vegf* (probe #405131) or human *VEGF* mRNA (probe #423161) vs. negative control (probe #320751). The signal was visualized and captured by a Zeiss confocal microscope meta 710 LSM (Carl Zeiss Inc.).

Immunohistochemistry

Immunohistochemical detection was performed according to the manufacturer's protocol on cryopreserved human tissue sections (obtained from the Wilmer Eye Institute Ocular

Pathology Archives with approval from the Johns Hopkins School of Medicine Internal Review Board) by using a nitroblue tetrazolium development system as previously described (69, 70) according to the manufacturer's protocol on neovascular AMD disease patients. Images were captured by scanning slides using the Aperio ScanScope program on Aperio Scanscope XT® System (Leica Biosystems, Wetzlar, Germany).

Immunofluorescence

Antibodies and dilutions are listed in Supplemental Table 5.

The immunofluorescence for the laser CNV model were performed on choroidal flat mounts and cross sections were performed as previously described (37). For choroidal flat mounts, eyes were enucleated and fixed in 4% paraformaldehyde solution (Thermo Scientific™) in PBS for 2 hours at room temperature or overnight at 4°C followed by washing with PBS 3 times for 10 minutes in a shaker. RPE/choroid was isolated and incubated in 0.5% BSA solution overnight at 4°C. They were then washed with PBS 3 times for 10 minutes in a shaker. HypoxyProbe was incubated with the flat mount retina at the indicated time points. Isolectin B4 (Invitrogen) or CD31 was used to label the choroidal vasculature and incubated overnight in 4°C. After 3 washes with PBS for 10 minutes each in a shaker, choroidal flat mounts were prepared. Images were captured at high magnification (20X) with Zeiss fluorescent microscope (Carl Zeiss Inc.) and the area of CNV lesions was calculated as mm^2 by image J software by keeping the parameters the same for all the spots.

For cross sections, eyes were fixed in 4% paraformaldehyde for 2 hours. After washing in PBS, the tissues were embedded in OCT containing 6% agarose (w/v) and 10-µm-thick slices were cut. Cross-sections were taken through laser-induced CNV lesions and stained with CD31;

labeling of retinal vasculature was used as an anatomical landmark for the presence or absence or vessels.

For double-labeling, samples were incubated in a blocking solution with 5% normal donkey serum plus 0.3% Triton X-100 in saline for 1 hour at room temperature (RT). Subsequently, the samples were incubated in a mixture of primary antibodies overnight at 4°C. After washing, the slices were incubated in secondary antibodies for 1 hour at RT.

Immunofluorescence was performed using donkey anti-mouse Alexa Fluor 488/555, donkey anti-goat Alexa Fluor 647 or donkey anti-rabbit Alexa Fluor 488/555, in combination with DAPI (Invitrogen). Images were captured by the LSM 710 confocal microscope (Carl Zeiss Inc., Thornwood, NY) or the EVOS FL Auto 2 Imaging System (Thermo Fisher Scientific, Waltham, MA).

Nanoparticles

Reducible branched ester amine quadpolymers (rBEAQs) were synthesized as previously described (46). Briefly, bioreducible monomer 2,2-disulfanediylbis(ethane-2,1-diyl) diacrylate (BR6), diacrylate monomer bisphenol A glycerolate (1 glycerol/phenol) diacrylate (B7), tri-acrylate monomer trimethylolpropane triacrylate (B8), and side chain monomer 4-amino-1-butanol (S4) were reacted overnight at 90°C with stirring to form the acrylate-terminated base polymer, which was then end-capped with 2-(3-aminopropylamino)ethanol (E6) to form the final polymer used in these studies (Fig. 7A; Supplemental Fig. 2). siRNA-encapsulating nanoparticles were formed by dissolving siRNA and polymer at the desired concentrations in 25 mM sodium acetate solution (NaAc; pH 5) and mixing the two solutions at a 1:1 volume ratio. Nanoparticles were allowed to self-assemble for 10 minutes at room temperature, at which time

they were mixed at a 1:1 volume ratio with sodium bicarbonate solution at a final concentration of 9 mg/mL ($NaHCO_3$; pH 9). For in vitro transfections, nanoparticle solutions were added directly to cell culture media and incubated for 4 hours. Nanoparticles were formulated at a polymer: siRNA weight (wt/wt) ratio of 40; the final siRNA dose was 100 nM per well. For transfections simultaneously knocking down VEGF and ANGPTL4, siRNA targeting each sequence was pre-mixed at a 1:1 molar ratio prior to mixing with polymers; siRNA dose in this case was 50 nM per well per siRNA sequence.

For intravitreal injections, nanoparticles were synthesized at a polymer concentration of 10 mg/mL to enable a higher dose to be delivered in the limited injection volume. Nanoparticles were lyophilized in the presence of sucrose (30 mg/mL) as a cryoprotectant and resuspended using deionized water to a final isotonic sucrose concentration of 100 mg/mL immediately prior to injection.

Patient Samples

Aqueous samples were collected from consenting patients with nvAMD at the Wilmer Eye Institute undergoing cataract and/or vitrectomy surgery or an intravitreal injection. Control samples were obtained from patients without nvAMD, diabetes mellitus, or retinal disease at the time of cataract surgery. At the time of intravitreal injection or cataract and/or vitrectomy surgery, aqueous was collected via limbal paracentesis using a 30-gauge needle attached to a tuberculin syringe. Aqueous samples were immediately processed and stored at -80°C prior to analysis.

ELISA

ANGPTL4 (DuoSet, cat# DY3485), VEGF (Quantikine, cat# DVE00), ANGPT2 (Quantikine, cat# DANG20) and sNRP1 (Quantikine, cat# DNRP10) enzyme-linked immunosorbent assay (ELISA) kits were purchased from R&D Systems. Aqueous fluid samples were diluted 1:10 and analyzed for ANGPTL4, VEGF, ANGPT2, or sNRP1 protein according to the manufacturer's protocols.

Statistical Analysis

In all non-clinical studies, results are shown as a mean value ± SD from at least three independent experiments. Results from clinical samples are shown as mean ± SD. Receiver operating characteristics (ROC) curves for each respective vasoactive mediator were generated using MATLAB. Statistical differences between groups was performed with Prism 8.0 software (GraphPad) and were determined by Kruskal-Wallis and Dunn's or Dunnett's T3 multiple comparisons tests, Wilcoxon matched-pairs signed rank test, two tailed Student's t test, One-way ANOVA with Bonferroni correction, chi-square test and Spearman correlation as indicated. Statistical significance was defined as P less than 0.05. *P<0.05; **P<0.01; ***P<0.001; ****P<0.0001; NS, nonsignificant.

Study Approval

All animals were treated in accordance with the Association for Research in Vision and Ophthalmology Statement for the Use of Animals in Ophthalmic and Vision Research and the guidelines of the Johns Hopkins University Animal Care and Use Committee.

Institutional Review Board approval from the Johns Hopkins University School of Medicine and informed consent were obtained for all patient samples used in this HIPAA-compliant study.

References

1. Harvey PT. Common eye diseases of elderly people: identifying and treating causes of vision loss. *Gerontology.* 2003;49(1):1-11.
2. Jager RD, Mieler WF, and Miller JW. Age-related macular degeneration. *The New England journal of medicine.* 2008;358(24):2606-17.
3. Nguyen DH, Luo J, Zhang K, and Zhang M. Current therapeutic approaches in neovascular age-related macular degeneration. *Discovery medicine.* 2013;15(85):343-8.
4. Spooner KL, Mhlanga CT, Hong TH, Broadhead GK, and Chang AA. The burden of neovascular age-related macular degeneration: a patient's perspective. *Clin Ophthalmol.* 2018;12:2483-91.
5. Malik D, Cao X, Sanchez JC, Gao T, Qian J, Montaner S, et al. Factors Associated With a Patient's Decision to Select a Cost-effective vs the Most Effective Therapy for Their Own Eye Disease. *JAMA Netw Open.* 2021;4(2):e2037880.
6. Li E, Donati S, Lindsley KB, Krzystolik MG, and Virgili G. Treatment regimens for administration of anti-vascular endothelial growth factor agents for neovascular age-related macular degeneration. *Cochrane Database Syst Rev.* 2020;5:CD012208.
7. Usui-Ouchi A, and Friedlander M. Anti-VEGF therapy: higher potency and long-lasting antagonism are not necessarily better. *J Clin Invest.* 2019;129(8):3032-4.
8. Cao X, Sanchez JC, Dinabandhu A, Guo C, Patel TP, Yang Z, et al. Aqueous proteins help predict the response of neovascular age-related macular degeneration patients to anti-VEGF therapy. *The Journal of Clinical Investigation.* 2022;132(2):e144469.

9. Kurihara T, Westenskow PD, and Friedlander M. Hypoxia-inducible factor (HIF)/vascular endothelial growth factor (VEGF) signaling in the retina. *Adv Exp Med Biol.* 2014;801:275-81.

10. Paulus YM, and Sodhi A. Anti-angiogenic Therapy for Retinal Disease. *Handb Exp Pharmacol.* 2017;242:271-307.

11. Arjamaa O, Nikinmaa M, Salminen A, and Kaarniranta K. Regulatory role of HIF-1alpha in the pathogenesis of age-related macular degeneration (AMD). *Ageing Res Rev.* 2009;8(4):349-58.

12. Lutty G, Grunwald J, Majji AB, Uyama M, and Yoneya S. Changes in choriocapillaris and retinal pigment epithelium in age-related macular degeneration. *Mol Vis.* 1999;5:35.

13. Stefansson E, Geirsdottir A, and Sigurdsson H. Metabolic physiology in age related macular degeneration. *Prog Retin Eye Res.* 2011;30(1):72-80.

14. Vadlapatla RK, Vadlapudi AD, and Mitra AK. Hypoxia-inducible factor-1 (HIF-1): a potential target for intervention in ocular neovascular diseases. *Curr Drug Targets.* 2013;14(8):919-35.

15. Inoue Y, Yanagi Y, Matsuura K, Takahashi H, Tamaki Y, and Araie M. Expression of hypoxia-inducible factor 1alpha and 2alpha in choroidal neovascular membranes associated with age-related macular degeneration. *Br J Ophthalmol.* 2007;91(12):1720-1.

16. Sheridan CM, Pate S, Hiscott P, Wong D, Pattwell DM, and Kent D. Expression of hypoxia-inducible factor-1alpha and -2alpha in human choroidal neovascular membranes. *Graefes Arch Clin Exp Ophthalmol.* 2009;247(10):1361-7.

17. Yoshida T, Zhang H, Iwase T, Shen J, Semenza GL, and Campochiaro PA. Digoxin inhibits retinal ischemia-induced HIF-1alpha expression and ocular neovascularization.

FASEB journal : official publication of the Federation of American Societies for Experimental Biology. 2010;24(6):1759-67.

18. Lin M, Hu Y, Chen Y, Zhou KK, Jin J, Zhu M, et al. Impacts of hypoxia-inducible factor-1 knockout in the retinal pigment epithelium on choroidal neovascularization. *Invest Ophthalmol Vis Sci.* 2012;53(10):6197-206.
19. Semenza GL. Hypoxia-inducible factor 1 and cardiovascular disease. *Annu Rev Physiol.* 2014;76:39-56.
20. Campochiaro PA. Molecular pathogenesis of retinal and choroidal vascular diseases. *Prog Retin Eye Res.* 2015;49:67-81.
21. Lobov IB, Brooks PC, and Lang RA. Angiopoietin-2 displays VEGF-dependent modulation of capillary structure and endothelial cell survival in vivo. *Proc Natl Acad Sci U S A.* 2002;99(17):11205-10.
22. Oliner JD, Bready J, Nguyen L, Estrada J, Hurh E, Ma H, et al. AMG 386, a selective angiopoietin 1/2-neutralizing peptibody, inhibits angiogenesis in models of ocular neovascular diseases. *Invest Ophthalmol Vis Sci.* 2012;53(4):2170-80.
23. Rennel ES, Regula JT, Harper SJ, Thomas M, Klein C, and Bates DO. A human neutralizing antibody specific to Ang-2 inhibits ocular angiogenesis. *Microcirculation.* 2011;18(7):598-607.
24. Hera R, Keramidas M, Peoc'h M, Mouillon M, Romanet JP, and Feige JJ. Expression of VEGF and angiopoietins in subfoveal membranes from patients with age-related macular degeneration. *Am J Ophthalmol.* 2005;139(4):589-96.

25. Otani A, Takagi H, Oh H, Koyama S, Matsumura M, and Honda Y. Expressions of angiopoietins and Tie2 in human choroidal neovascular membranes. *Invest Ophthalmol Vis Sci.* 1999;40(9):1912-20.

26. De La Huerta I, Kim SJ, and Sternberg P, Jr. Faricimab Combination Therapy for Sustained Efficacy in Neovascular Age-Related Macular Degeneration. *JAMA Ophthalmol.* 2020;138(9):972-3.

27. Sharma A, Kumar N, Kuppermann BD, Bandello F, and Loewenstein A. Faricimab: expanding horizon beyond VEGF. *Eye (Lond).* 2020;34(5):802-4.

28. Heier JS, Khanani AM, Quezada Ruiz C, Basu K, Ferrone PJ, Brittain C, et al. Efficacy, durability, and safety of intravitreal faricimab up to every 16 weeks for neovascular age-related macular degeneration (TENAYA and LUCERNE): two randomised, double-masked, phase 3, non-inferiority trials. *The Lancet.* 2022;399(10326):729-40.

29. Nicolo M, Ferro Desideri L, Vagge A, and Traverso CE. Faricimab: an investigational agent targeting the Tie-2/angiopoietin pathway and VEGF-A for the treatment of retinal diseases. *Expert Opin Investig Drugs.* 2021;30(3):193-200.

30. Jonas JB, and Neumaier M. Erythropoietin levels in aqueous humour in eyes with exudative age-related macular degeneration and diabetic retinopathy. *Clin Exp Ophthalmol.* 2007;35(2):186-7.

31. Wang ZY, Zhao KK, Song ZM, Shen LJ, and Qu J. Erythropoietin as a novel therapeutic agent for atrophic age-related macular degeneration. *Med Hypotheses.* 2009;72(4):448-50.

32. Babapoor-Farrokhran S, Jee K, Puchner B, Hassan SJ, Xin X, Rodrigues M, et al. Angiopoietin-like 4 is a potent angiogenic factor and a novel therapeutic target for

patients with proliferative diabetic retinopathy. *Proceedings of the National Academy of Sciences of the United States of America.* 2015;112(23):E3030-9.

33. Jee K, Rodrigues M, Kashiwabuchi F, Applewhite BP, Han I, Lutty G, et al. Expression of the angiogenic mediator, angiopoietin-like 4, in the eyes of patients with proliferative sickle retinopathy. *PLoS One.* 2017;12(8):e0183320.

34. Xin X, Rodrigues M, Umapathi M, Kashiwabuchi F, Ma T, Babapoor-Farrokhran S, et al. Hypoxic retinal Muller cells promote vascular permeability by HIF-1-dependent up-regulation of angiopoietin-like 4. *Proceedings of the National Academy of Sciences of the United States of America.* 2013;110(36):E3425-34.

35. Bhutto I, and Lutty G. Understanding age-related macular degeneration (AMD): relationships between the photoreceptor/retinal pigment epithelium/Bruch's membrane/choriocapillaris complex. *Molecular aspects of medicine.* 2012;33(4):295-317.

36. Bhutto IA, McLeod DS, Hasegawa T, Kim SY, Merges C, Tong P, et al. Pigment epithelium-derived factor (PEDF) and vascular endothelial growth factor (VEGF) in aged human choroid and eyes with age-related macular degeneration. *Experimental eye research.* 2006;82(1):99-110.

37. Shah RS, Soetikno BT, Lajko M, and Fawzi AA. A Mouse Model for Laser-induced Choroidal Neovascularization. *J Vis Exp.* 2015(106):e53502.

38. Grossniklaus HE, Kang SJ, and Berglin L. Animal models of choroidal and retinal neovascularization. *Prog Retin Eye Res.* 2010;29(6):500-19.

39. Yu AY, Shimoda LA, Iyer NV, Huso DL, Sun X, McWilliams R, et al. Impaired physiological responses to chronic hypoxia in mice partially deficient for hypoxia-inducible factor 1alpha. *J Clin Invest.* 1999;103(5):691-6.

40. Bosch-Marce M, Okuyama H, Wesley JB, Sarkar K, Kimura H, Liu YV, et al. Effects of aging and hypoxia-inducible factor-1 activity on angiogenic cell mobilization and recovery of perfusion after limb ischemia. *Circ Res.* 2007;101(12):1310-8.

41. Sodhi A, Ma T, Menon D, Deshpande M, Jee K, Dinabandhu A, et al. Angiopoietin-like 4 binds neuropilins and cooperates with VEGF to induce diabetic macular edema. *J Clin Invest.* 2019;129(11):4593-608.

42. Sodhi A, and Montaner S. Angiopoietin-like 4 as an Emerging Therapeutic Target for Diabetic Eye Disease. *JAMA ophthalmology.* 2015;133(12):1375-6.

43. Ye X, Wang Y, Cahill H, Yu M, Badea TC, Smallwood PM, et al. Norrin, frizzled-4, and Lrp5 signaling in endothelial cells controls a genetic program for retinal vascularization. *Cell.* 2009;139(2):285-98.

44. Okamoto N, Tobe T, Hackett SF, Ozaki H, Vinores MA, LaRochelle W, et al. Transgenic mice with increased expression of vascular endothelial growth factor in the retina: a new model of intraretinal and subretinal neovascularization. *Am J Pathol.* 1997;151(1):281-91.

45. Zhang J, Qin Y, Martinez M, Flores-Bellver M, Rodrigues M, Dinabandhu A, et al. HIF-1alpha and HIF-2alpha redundantly promote retinal neovascularization in patients with ischemic retinal disease. *J Clin Invest.* 2021;131(12):e139202.

46. Rui Y, Wilson DR, Sanders K, and Green JJ. Reducible Branched Ester-Amine Quadpolymers (rBEAQs) Codelivering Plasmid DNA and RNA Oligonucleotides Enable CRISPR/Cas9 Genome Editing. *ACS Appl Mater Interfaces.* 2019;11(11):10472-80.

47. Parker MW, Guo HF, Li X, Linkugel AD, and Vander Kooi CW. Function of members of the neuropilin family as essential pleiotropic cell surface receptors. *Biochemistry.* 2012;51(47):9437-46.

48. Gagnon ML, Bielenberg DR, Gechtman Z, Miao HQ, Takashima S, Soker S, et al. Identification of a natural soluble neuropilin-1 that binds vascular endothelial growth factor: In vivo expression and antitumor activity. *Proc Natl Acad Sci U S A.* 2000;97(6):2573-8.

49. Pellet-Many C, Frankel P, Jia H, and Zachary I. Neuropilins: structure, function and role in disease. *Biochem J.* 2008;411(2):211-26.

50. Miller JW, Le Couter J, Strauss EC, and Ferrara N. Vascular endothelial growth factor a in intraocular vascular disease. *Ophthalmology.* 2013;120(1):106-14.

51. Ferrara N. Vascular endothelial growth factor and age-related macular degeneration: from basic science to therapy. *Nature medicine.* 2010;16(10):1107-11.

52. Kelly BD, Hackett SF, Hirota K, Oshima Y, Cai Z, Berg-Dixon S, et al. Cell type-specific regulation of angiogenic growth factor gene expression and induction of angiogenesis in nonischemic tissue by a constitutively active form of hypoxia-inducible factor 1. *Circulation research.* 2003;93(11):1074-81.

53. Tolentino MJ, Miller JW, Gragoudas ES, Jakobiec FA, Flynn E, Chatzistefanou K, et al. Intravitreous injections of vascular endothelial growth factor produce retinal ischemia and microangiopathy in an adult primate. *Ophthalmology.* 1996;103(11):1820-8.

54. Ozaki H, Hayashi H, Vinores SA, Moromizato Y, Campochiaro PA, and Oshima K. Intravitreal sustained release of VEGF causes retinal neovascularization in rabbits and breakdown of the blood-retinal barrier in rabbits and primates. *Experimental eye research.* 1997;64(4):505-17.

55. Ohno-Matsui K, Hirose A, Yamamoto S, Saikia J, Okamoto N, Gehlbach P, et al. Inducible expression of vascular endothelial growth factor in adult mice causes severe

proliferative retinopathy and retinal detachment. *The American journal of pathology.* 2002;160(2):711-9.

56. Khan M, Aziz AA, Shafi NA, Abbas T, and Khanani AM. Targeting Angiopoietin in Retinal Vascular Diseases: A Literature Review and Summary of Clinical Trials Involving Faricimab. *Cells.* 2020;9(8):1869.

57. Khanani AM, Patel SS, Ferrone PJ, Osborne A, Sahni J, Grzeschik S, et al. Efficacy of Every Four Monthly and Quarterly Dosing of Faricimab vs Ranibizumab in Neovascular Age-Related Macular Degeneration: The STAIRWAY Phase 2 Randomized Clinical Trial. *JAMA Ophthalmol.* 2020;138(9):964-72.

58. Sahni J, Dugel PU, Patel SS, Chittum ME, Berger B, Del Valle Rubido M, et al. Safety and Efficacy of Different Doses and Regimens of Faricimab vs Ranibizumab in Neovascular Age-Related Macular Degeneration: The AVENUE Phase 2 Randomized Clinical Trial. *JAMA Ophthalmol.* 2020;138(9):955-63.

59. Ma T, Jham BC, Hu J, Friedman ER, Basile JR, Molinolo A, et al. Viral G protein-coupled receptor up-regulates Angiopoietin-like 4 promoting angiogenesis and vascular permeability in Kaposi's sarcoma. *Proceedings of the National Academy of Sciences of the United States of America.* 2010;107(32):14363-8.

60. Kersten S. Role and mechanism of the action of angiopoietin-like protein ANGPTL4 in plasma lipid metabolism. *J Lipid Res.* 2021;62:100150.

61. Guo L, Li SY, Ji FY, Zhao YF, Zhong Y, Lv XJ, et al. Role of Angptl4 in vascular permeability and inflammation. *Inflamm Res.* 2014;63(1):13-22.

62. Landowski M, and Bowes Rickman C. Targeting Lipid Metabolism for the Treatment of Age-Related Macular Degeneration: Insights from Preclinical Mouse Models. *J Ocul Pharmacol Ther.* 2022;38(1):3-32.

63. Whitcup SM, Sodhi A, Atkinson JP, Holers VM, Sinha D, Rohrer B, et al. The role of the immune response in age-related macular degeneration. *Int J Inflam.* 2013;2013:348092.

64. Kim JH, Shin JP, Kim IT, and Park DH. Angiopoietin-Like 4 Correlates with Response to Intravitreal Ranibizumab Injections in Neovascular Age-Related Macular Degeneration. *Retina.* 2018;38(3):523-30.

65. Heier JS, Brown DM, Shah SP, Saroj N, Dang S, Waheed NK, et al. Intravitreal Aflibercept Injection vs Sham as Prophylaxis Against Conversion to Exudative Age-Related Macular Degeneration in High-risk Eyes: A Randomized Clinical Trial. *JAMA Ophthalmol.* 2021;139(5):542-7.

66. Guo HF, and Vander Kooi CW. Neuropilin Functions as an Essential Cell Surface Receptor. *J Biol Chem.* 2015;290(49):29120-6.

67. Gavard J, and Gutkind JS. VEGF controls endothelial-cell permeability by promoting the beta-arrestin-dependent endocytosis of VE-cadherin. *Nat Cell Biol.* 2006;8(11):1223-34.

68. Smith LE, Wesolowski E, McLellan A, Kostyk SK, D'Amato R, Sullivan R, et al. Oxygen-induced retinopathy in the mouse. *Investigative ophthalmology & visual science.* 1994;35(1):101-11.

69. Montaner S, Sodhi A, Molinolo A, Bugge TH, Sawai ET, He Y, et al. Endothelial infection with KSHV genes in vivo reveals that vGPCR initiates Kaposi's sarcomagenesis and can promote the tumorigenic potential of viral latent genes. *Cancer cell.* 2003;3(1):23-36.

70. Rodrigues M, Kashiwabuchi F, Deshpande M, Jee K, Goldberg MF, Lutty G, et al. Expression Pattern of HIF-1alpha and VEGF Supports Circumferential Application of Scatter Laser for Proliferative Sickle Retinopathy. *Invest Ophthalmol Vis Sci.* 2016;57(15):6739-46.

Acknowledgments

This work was supported by National Eye Institute, National Institutes of Health grants R01EY029750 to A.S., R01EY025705 to S.M. and A.S., R01EY031097 to J.J.G., and EY001765 (the Wilmer Core Grant for Vision Research, Microscopy and Imaging Core Module). A.S. gratefully acknowledges the support he received as a Special Scholar Award recipient from Research to Prevent Blindness, Inc., as recipient of the Alcon Young Investigator Award from the Alcon Research Institute, and from the Branna and Irving Sisenwein Professorship in Ophthalmology. G.L.S. is a recipient of the Sybil B. Harrington Stein Innovation Award for Macular Degeneration from Research to Prevent Blindness, Inc.

Figure 1

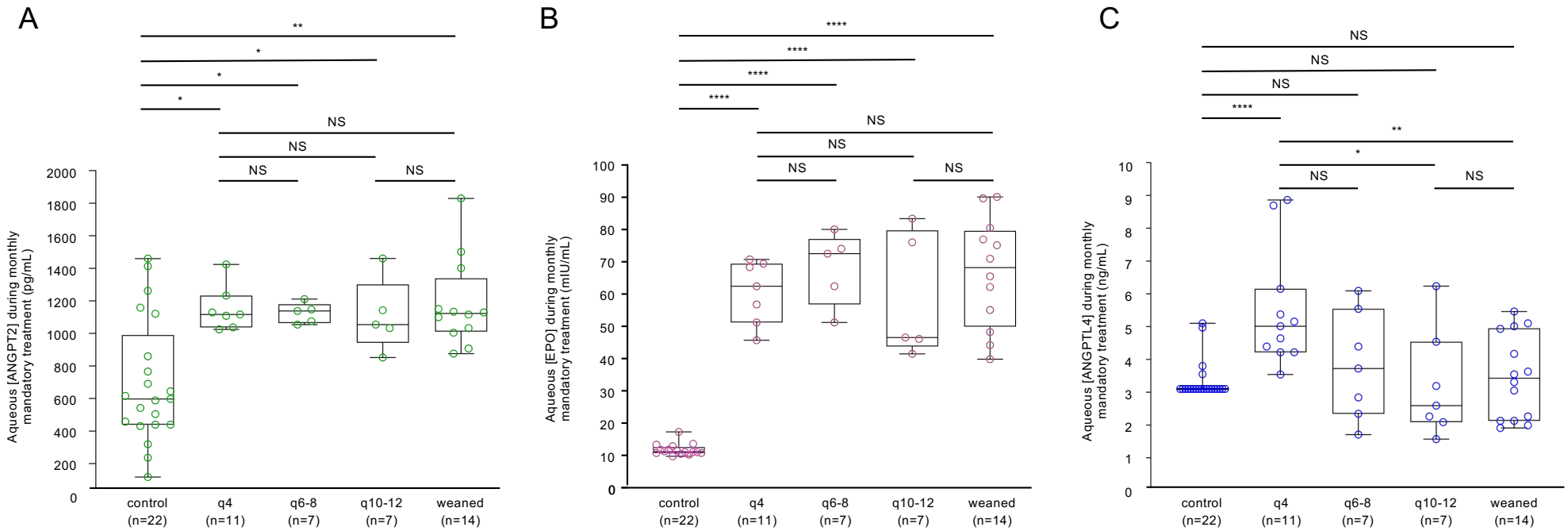
A
B
C
Aqueous [ANGPT2] during monthly mandatory treatment (pg/mL)
Aqueous [EPO] during monthly mandatory treatment (mIU/mL)
Aqueous [ANGPTL4] during monthly mandatory treatment (ng/mL)
control (n=22)
q4 (n=11)
q6-8 (n=7)
q10-12 (n=7)
weaned (n=14)
NS
*
**
****

Figure 1. Aqueous levels of HIF-regulated vasoactive mediators, ANGPT2, EPO, and ANGPTL4 in patients with nvAMD treated with anti-VEGF therapy.

(**A-C**) Aqueous ANGPT2 (A), EPO (B), and ANGPTL4 (C) levels of patients during initial 3 monthly mandatory treatment phase of a treat-and-extend protocol for patients with increasing interval between treatments at 12 months [from subset of TEP/M patients divided into groups based on the required treatment interval at the end of year 1 using the TEP/M protocol to wean patients from treatment (1)]. Patients extended to 12 weeks had treatment paused and patients were considered "weaned" off treatment if treatment pause reached 30 weeks. Statistical analysis was performed using Wilcoxon rank sum test. control, non-AMD eyes; q4, patients requiring treatment every 4 weeks; q6-8, patients requiring treatment every 6-8 weeks; q6-8, patients requiring treatment every 10-12 weeks; weaned, patients who were successfully weaned off treatment with anti-VEGF therapy. *$P < 0.05$; **$P < 0.01$; ***$P < 0.001$; ****$P < 0.0001$. NS, not significant.

Figure 2

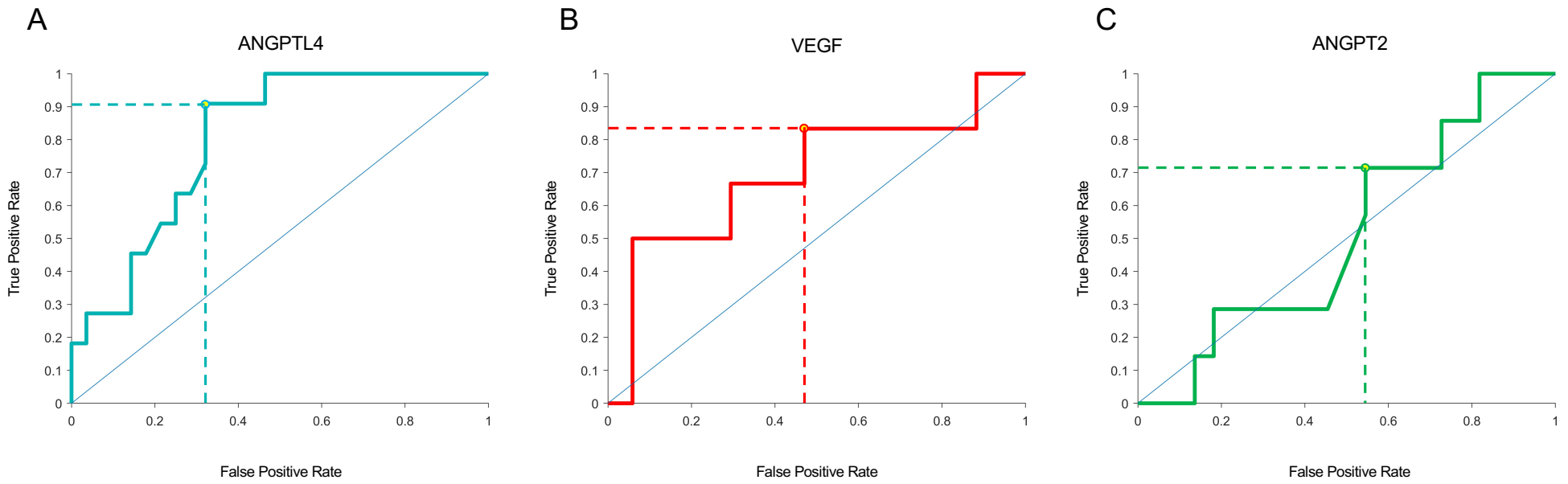
A
ANGPTL4
True Positive Rate
False Positive Rate
B
VEGF
True Positive Rate
False Positive Rate
C
ANGPT2
True Positive Rate
False Positive Rate

Figure 2. Receiver operating characteristic (ROC) curves for HIF-regulated vasoactive mediators in TEP/M patients when predicting patients who required monthly treatment with anti-VEGF for (A) VEGF, (B) ANGPT2, and (C) ANGPTL4. Optimal predictive values are denoted by the yellow marker and dashed lines based on selected cutoff concentrations for each mediator: VEGF, 260 pg/mL; ANGPT2, 1,100 pg/mL; and ANGPTL4, 4.22 ng/mL.

Figure 3

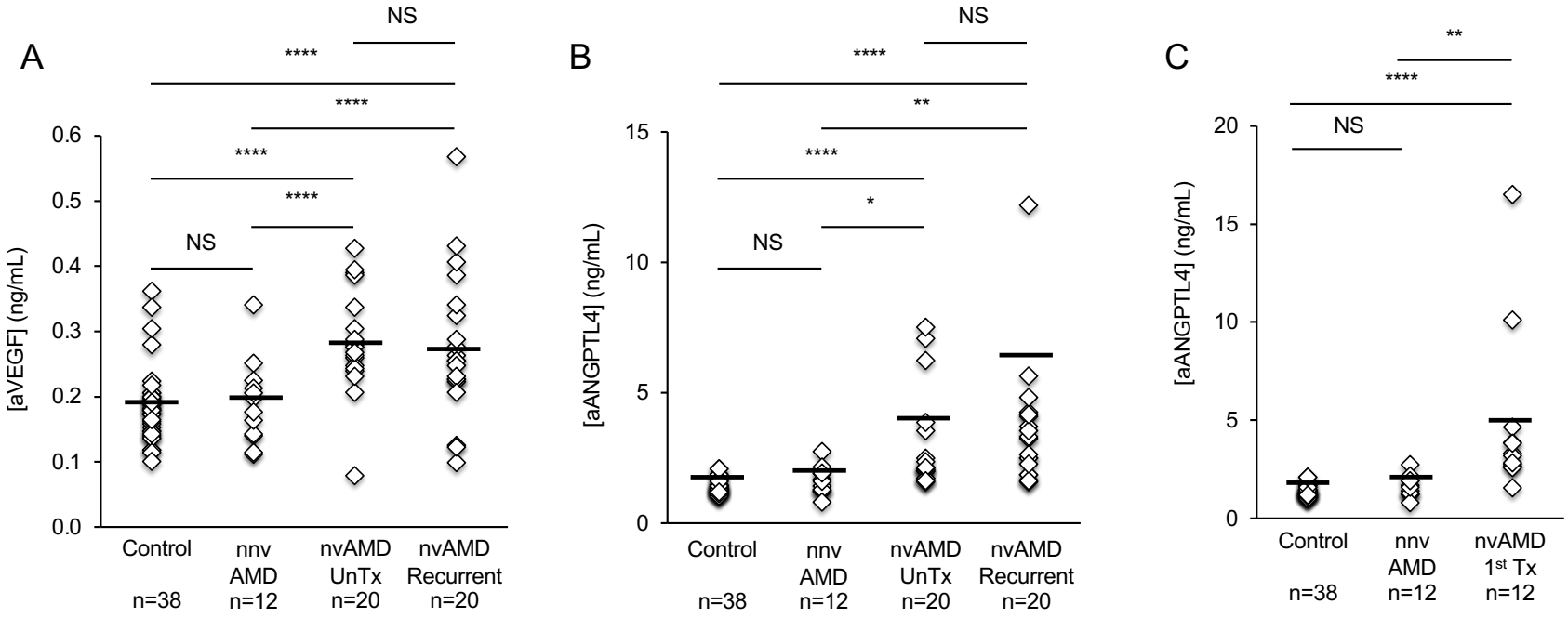
A
B
C
[aVEGF] (ng/mL)
[aANGPTL4] (ng/mL)
[aANGPTL4] (ng/mL)
NS
****
**
*
Control
n=38
nnv AMD
n=12
nvAMD UnTx
n=20
nvAMD Recurrent
n=20
nvAMD 1st Tx
n=12

Figure 3. Expression of VEGF and ANGPTL4 in aqueous fluid from nvAMD patients treated in the clinic for active CNV.

(**A** and **B**) Aqueous levels of VEGF (A) and ANGPTL4 (B) in treatment-naïve patients with active nvAMD (i.e., nvAMD patients who have never received anti-VEGF therapy; nvAMD UnTx) and patients with nvAMD previously treated with anti-VEGF therapy 12 or more weeks prior to sample collection (nvAMD Recurrent) compared to patients with nnvAMD and non-AMD (Control) patients. NOTE: Aqueous samples with [ANGPTL4] > 15 ng/mL are not displayed to adequately demonstrate the variability within the nvAMD samples; see Supplemental Figure 1A and B for all samples tested. (**C**) Aqueous levels of ANGPTL4 in patients with nvAMD treated with their first anti-VEGF therapy within 4-6 weeks of sample collection (nvAMD 1st Tx) compared to patients with nnvAMD and non-AMD (Control) patients. Kruskal-Wallis with Dunn's multiple comparisons test, *P < 0.05; **P < 0.01; ***P < 0.001; ****P < 0.0001; NS, not significant.

Figure 4

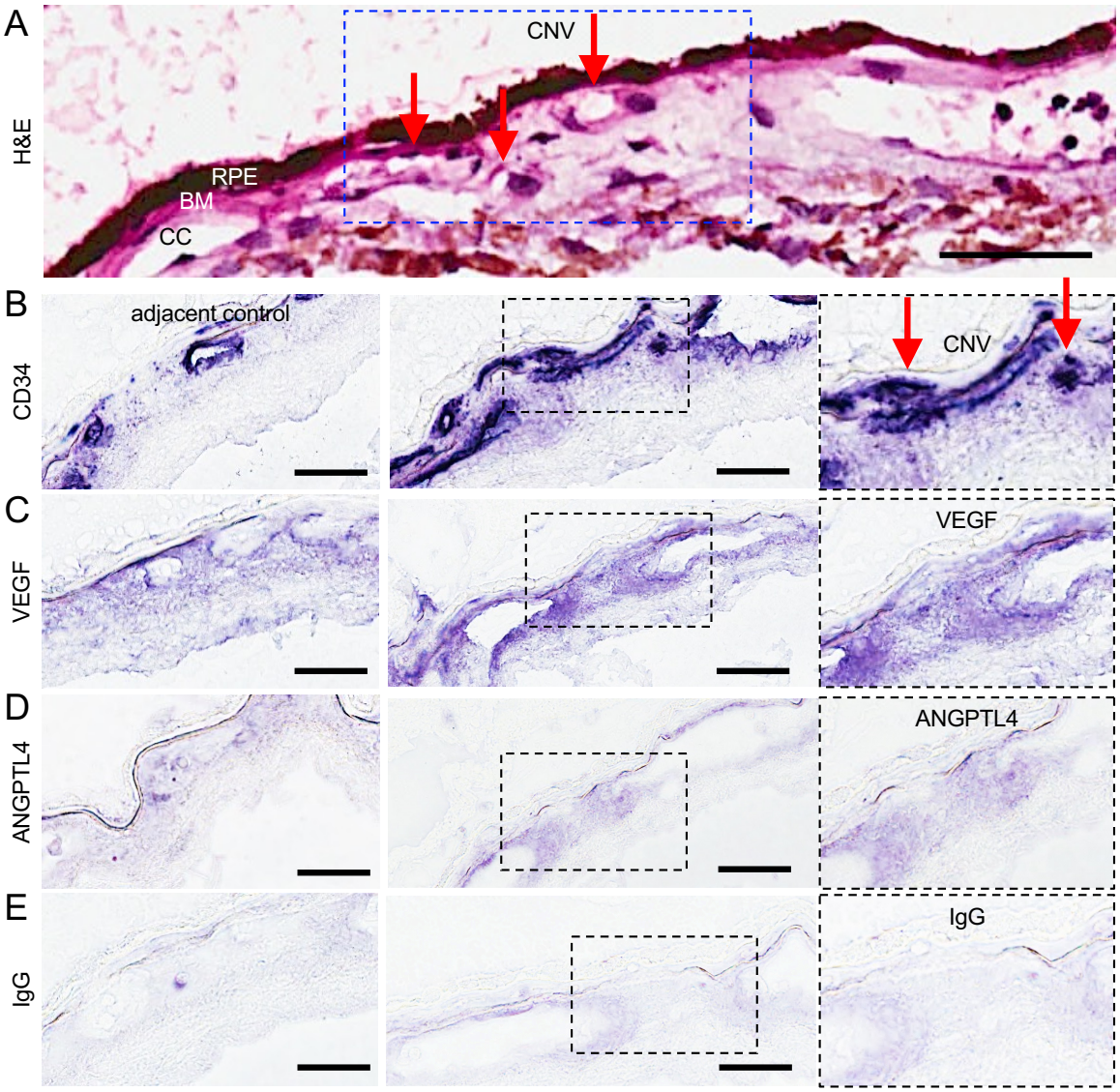
A
H&E
CNV
RPE
BM
CC
B
CD34
adjacent control
CNV
C
VEGF
VEGF
D
ANGPTL4
ANGPTL4
E
IgG
IgG

Figure 4. Expression of VEGF and ANGPTL4 in autopsy eyes from patients with known nvAMD.

(**A**) Representative images from hematoxylin and eosin (H&E) staining of a CNV lesion in an autopsy eye from a patient with known nvAMD. Red arrows point to CNV vessels that have broken through (and are anterior to) Bruch's membrane (BM). **(B)** Representative images from immunohistochemical analysis for CD31 within the area of the CNV membrane (CNV; *right*) or adjacent tissue without active CNV (adjacent control; *left*). **(C** and **D**) Representative images from immunohistochemical analysis for VEGF and ANGPTL4 within the area of the CNV membrane or in adjacent control. Inset demonstrates magnified view of staining within CNV lesion. (**E**) IgG is used as a negative control. RPE = retinal pigment epithelium; BM = Bruch's membrane; CC = choriocapillaris. Scale bars = 25 μm.

Figure 5

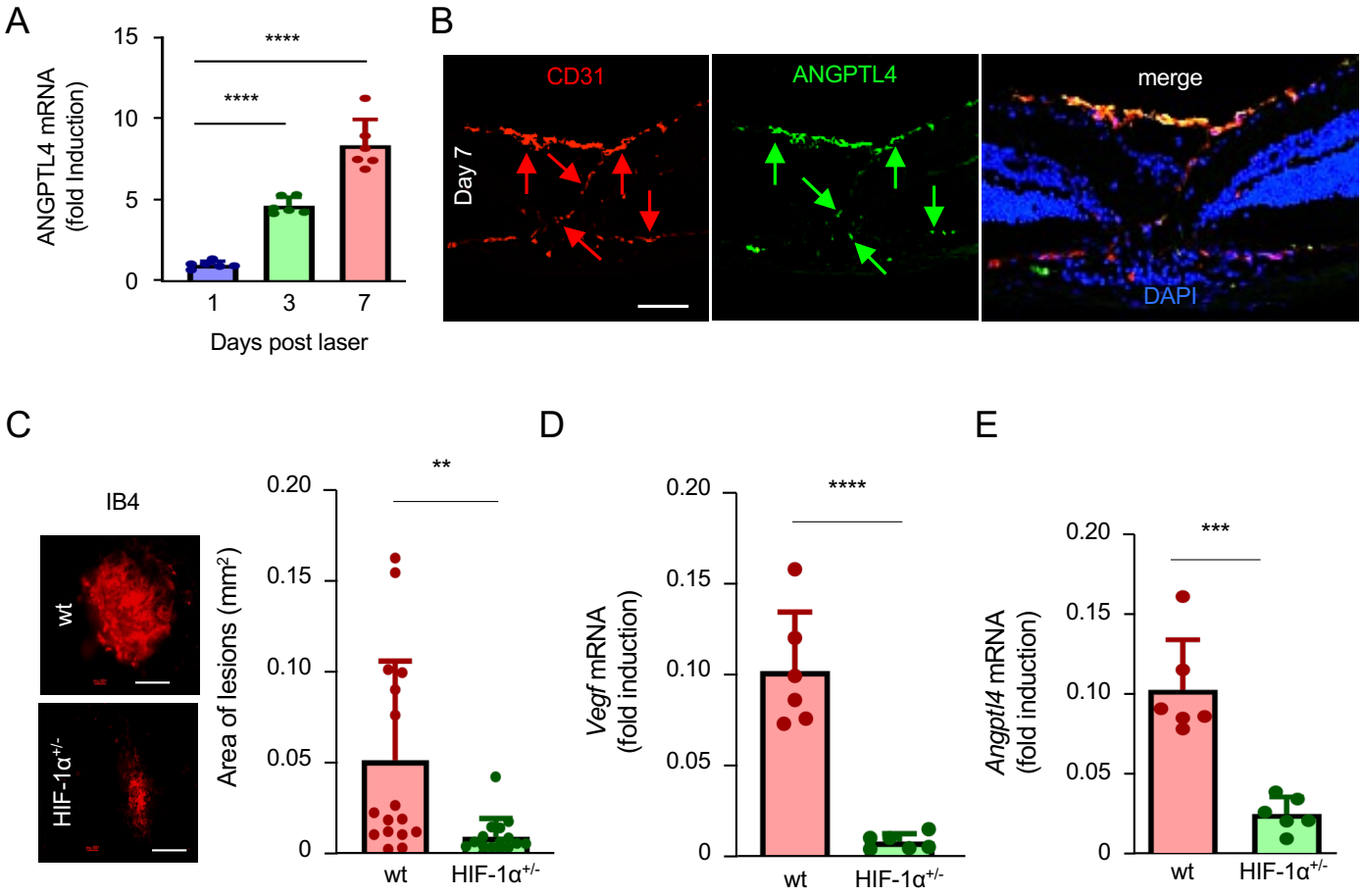
A
ANGPTL4 mRNA (fold Induction)
15
10
5
0
****
****
1
3
7
Days post laser
B
CD31
ANGPTL4
merge
Day 7
DAPI
C
IB4
wt
HIF-1α+/-
Area of lesions (mm2)
0.20
0.15
0.10
0.05
0
**
wt
HIF-1α+/-
D
Vegf mRNA (fold induction)
0.20
0.15
0.10
0.05
0
****
wt
HIF-1α+/-
E
Angptl4 mRNA (fold induction)
0.20
0.15
0.10
0.05
0
***
wt
HIF-1α+/-

Figure 5. HIF-dependent expression of ANGPTL4 in in laser-induced CNV lesions in mice. (**A**) Expression of *Angptl4* mRNA (qPCR) in RPE/choroidal lysates from laser CNV eyes over time. (**B**) Expression of ANGPTL4 protein (green arrows) in laser CNV lesions (labeled with CD31; red arrows) 7 days following laser treatment. (**C**) Size of CNV lesions in *Hif1a*$^{+/-}$ mice compared to wt littermate controls. (**D** and **E**) Expression of *Vegf* (D) and *Angptl4* (E) mRNA (qPCR) in RPE/choroidal lysates from laser CNV eyes in *Hif1a*$^{+/-}$ mice compared to wt littermate controls. n=3-6 animals. Blue nuclear staining with DAPI. Scale bars = 60 μm (B) or 200 μm (C). Student's t-test, *P < 0.05; **P < 0.01; ***P < 0.001; ****P < 0.0001; NS, non-significant.

Figure 6

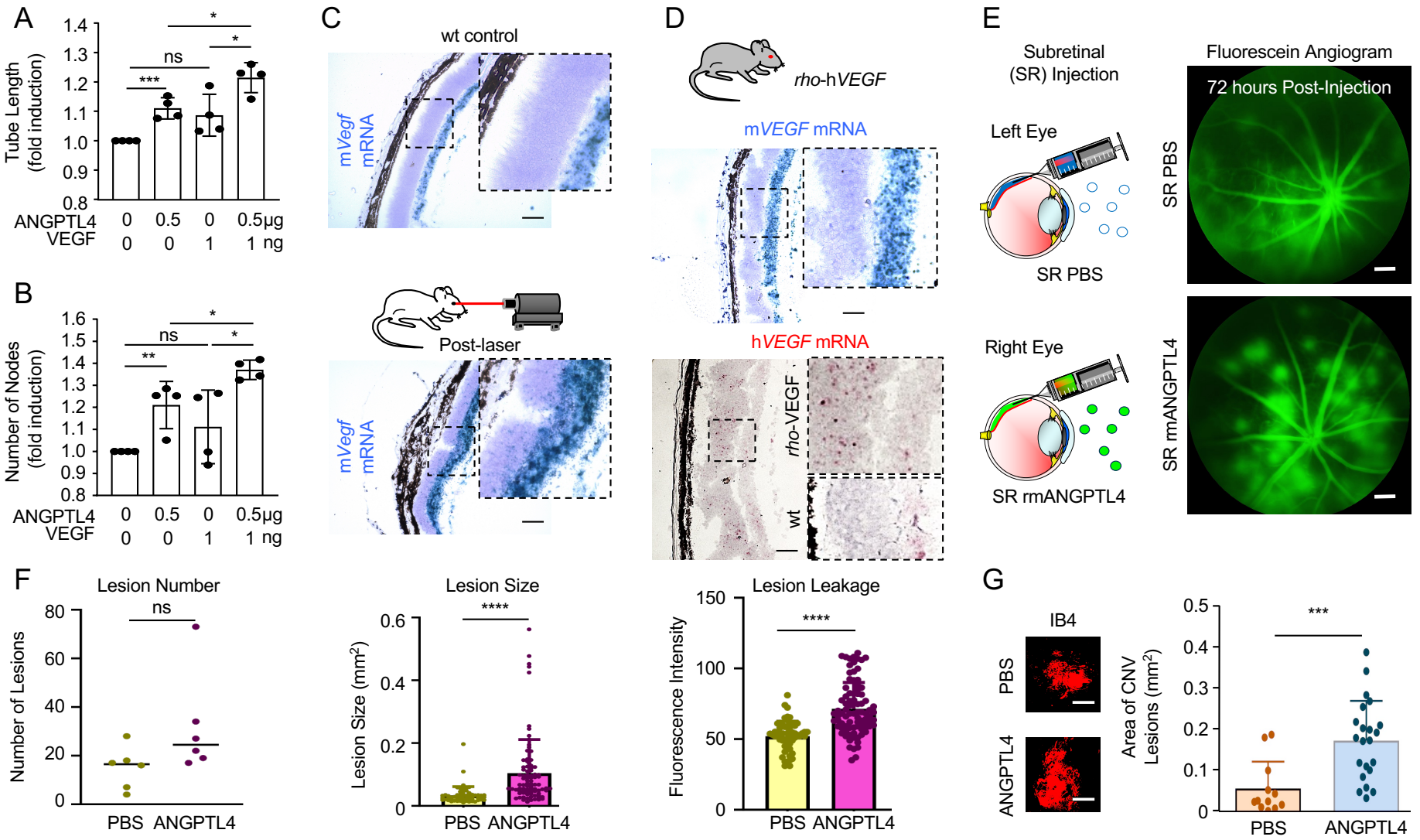
A
Tube Length (fold induction)
ANGPTL4
VEGF
B
Number of Nodes (fold induction)
C
wt control
mVegf mRNA
Post-laser
D
rho-hVEGF
mVEGF mRNA
hVEGF mRNA
rho-VEGF
wt
E
Subretinal (SR) Injection
Left Eye
SR PBS
Right Eye
SR rmANGPTL4
Fluorescein Angiogram
72 hours Post-Injection
F
Lesion Number
Number of Lesions
Lesion Size
Lesion Size (mm²)
Lesion Leakage
Fluorescence Intensity
G
IB4
PBS
ANGPTL4
Area of CNV Lesions (mm²)

Figure 6. ANGPTL4 enhances the ability of VEGF to promote CNV lesions in mice.

(**A** and **B**) Endothelial cell tubule length (A) and number of nodes (B) in response to treatment with rhANGPTL4, rhVEGF, or both. (**C**) Expression of murine *Vegf* (m*Vegf*) mRNA (in situ hybridization) in control (wt) animals (*above*) and 7 days following treatment with laser (*below*). (**D**) Expression of m*Vegf* (blue) and human *VEGF* (h*VEGF*; red) mRNA in *rho*-h*VEGF* transgenic mice. (**E**) Schematic (*left*) demonstrating subretinal injection with PBS (*above*) or recombinant murine ANGPTL4 (rmANGPTL4; *below*) in *rho*-h*VEGF* mice. Fluorescein angiogram (FA; *right*) demonstrating fluorescein leakage from CNV lesions 72 hours following subretinal injection of PBS (*above*) or rmANGPTL4 (*below*). (**F**) The number (*left*) and size (*middle*) of, and leakage from (*right*) CNV lesions on FA. (**G**) Size of CNV lesions on choroidal flat mounts stained with isolectin 72 hours after following subretinal injection of PBS or rmANGPTL4. n=6-9 animals. Scale bars = 100 μm for C and D (above) and 200 μm D (below), E, and G. Wilcoxon signed-rank test and Student's t-test, *P < 0.05; **P < 0.01; ***P < 0.001; ****P < 0.0001; NS, non-significant.

Figure 7

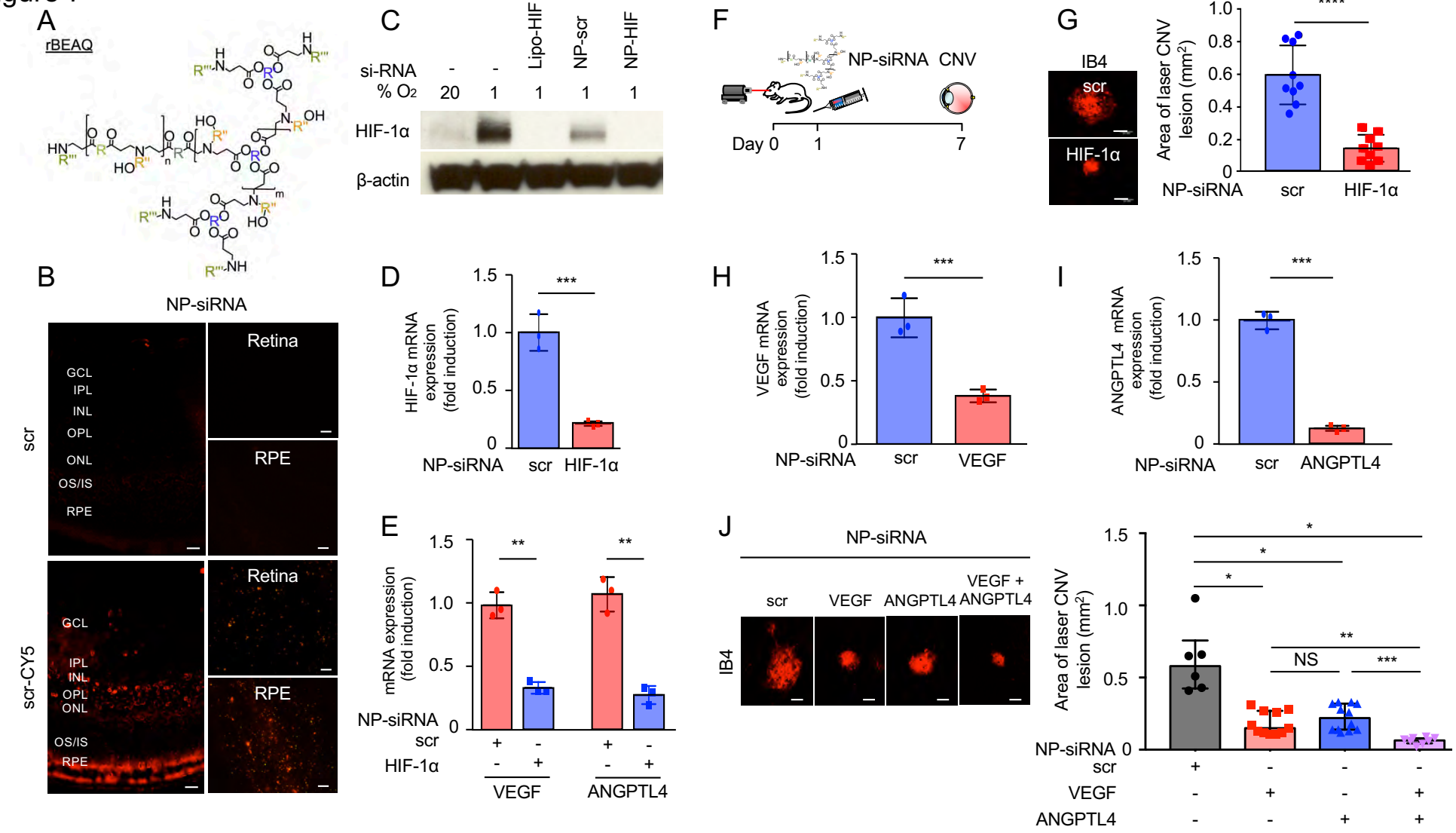
A
rBEAQ
B
NP-siRNA
scr
scr-CY5
Retina
RPE
GCL
IPL
INL
OPL
ONL
OS/IS
RPE
C
si-RNA
% O2
Lipo-HIF
NP-scr
NP-HIF
HIF-1α
β-actin
D
HIF-1α mRNA expression (fold induction)
NP-siRNA
scr
HIF-1α
E
mRNA expression (fold induction)
NP-siRNA
scr
HIF-1α
VEGF
ANGPTL4
F
NP-siRNA
CNV
Day 0
1
7
G
IB4
scr
HIF-1α
Area of laser CNV lesion (mm2)
NP-siRNA
scr
HIF-1α
H
VEGF mRNA expression (fold induction)
NP-siRNA
scr
VEGF
I
ANGPTL4 mRNA expression (fold induction)
NP-siRNA
scr
ANGPTL4
J
NP-siRNA
scr
VEGF
ANGPTL4
VEGF + ANGPTL4
IB4
Area of laser CNV lesion (mm2)
NS
NP-siRNA
scr
VEGF
ANGPTL4

Figure 7. In vivo nanoparticle-mediated siRNA targeting ANGPTL4 and VEGF more effective than targeting either angiogenic factor alone for the treatment of laser CNV mice. (**A**) rBEAQ polymer for in vivo delivery of siRNA. (**B**) Expression of fluorophore in cross section (*left*) and neurosensory retina (Retina) or RPE/choroidal (RPE) flat mounts (*right*) of mice 1 day following intravitreal injection with NP-scr or NP-scr conjugated to Cy5. (**C**) Expression of HIF-1α protein (WB) in lysates from 1° mouse RPE cells treated with 1% O_2 in the presence of nanoparticle-encapsulated siRNA targeting *Hif1a* (NP-HIF) vs. scrambled control (NP-scr) for 72 hours. Standard transfection with Lipofectamine RNAiMAX-encapsulated siRNA targeting *Hif1a* (Lipo-HIF) was used as a positive control. (**D** and **E**) *Hif1a* (D) *Vegf* and *Angptl4* (E) mRNA expression (qPCR) in RPE/choroidal lysates 5 days following a single intravitreal injection with siRNA targeting *Hif1a* (NP-HIF) vs. NP-scr in mice. (**F**) Schematic of Laser CNV model in which a single dose of NP-HIF or NP-scr control is administered by intravitreal injection 1 day after laser treatment; eyes were enucleated for analysis on day 7. (**G**) Size of CNV lesion in mice treated with NP-scr or NP-HIF. (**H** and **I**) *Vegf* (H) and *Angptl4* (I) mRNA expression (qPCR) in RPE/choroidal lysates 5 days following a single intravitreal injection with siRNA targeting *Vegf* (NP-VEGF) or *Angptl4* (NP-ANGPTL4), respectively. (**J**) Size of CNV lesion in mice treated with NP-scr, NP-VEGF, NP-ANGPTL4, or both NP-VEGF and NP-ANGPTL4 administered by intravitreal injection 1 day after laser treatment; eyes were enucleated for analysis on day 7. n = 3-6 animals. GCL = ganglion cell layer; IPL = inner plexiform layer; INL = inner nuclear layer; OPL = outer plexiform layer; ONL = outer nuclear layer; IS/OS = inner/outer segments; RPE = retinal pigment epithelium. Scale bars = 25 μm for B and 100 μm for G and J. Student's t test (D, E, G, H and I), and Kruskal-Wallis with Dunnett's T3 correction (J), *P < 0.05; **P < 0.01; ***P < 0.001; ****P < 0.0001;

NS, non-significant.

Figure 8

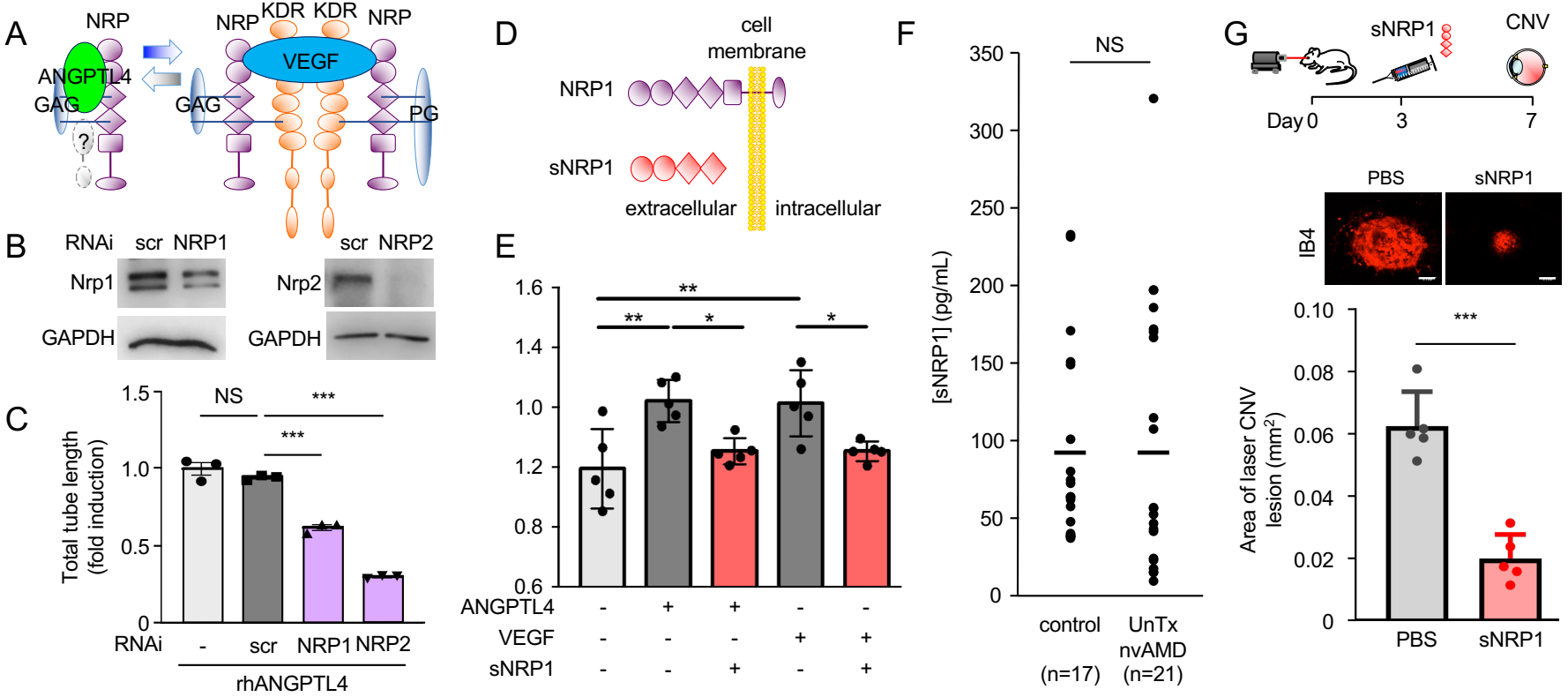
A
NRP
NRP
KDR
KDR
NRP
VEGF
ANGPTL4
GAG
GAG
PG
?
B
RNAi
scr
NRP1
scr
NRP2
Nrp1
Nrp2
GAPDH
GAPDH
C
Total tube length (fold induction)
NS
***
***
1.5
1.0
0.5
0
RNAi
-
scr
NRP1
NRP2
rhANGPTL4
D
cell membrane
NRP1
sNRP1
extracellular
intracellular
E
1.6
1.4
1.2
1.0
0.8
0.6
**
**
*
*
ANGPTL4
VEGF
sNRP1
F
[sNRP1] (pg/mL)
NS
350
300
250
200
150
100
50
0
control (n=17)
UnTx nvAMD (n=21)
G
sNRP1
CNV
Day 0
3
7
PBS
sNRP1
IB4
Area of laser CNV lesion (mm²)
***
0.10
0.08
0.06
0.04
0.02
0
PBS
sNRP1

Figure 8: sNRP1 reduces the promotion of angiogenesis by ANGPTL4 and inhibits CNV in mice.

(**A**) Schematic demonstrating binding of ANGPTL4 and VEGF to the endothelial cell receptors, neuropilin (NRP)1 and NRP2. (**B** and **C**) Knock down of NRP1 or NRP2 (B) inhibits the promotion of human umbilical vein endothelial cell (HUVEC) tubule formation by rhANGPTL4 (C). (**D**) Schematic comparing NRP1 and sNRP1; the latter lacks the transmembrane domain and is therefore soluble. (**E**) sNRP1 inhibits the promotion of iREC tubule formation by rhANGPTL4 and rhVEGF. (**F**) Expression of sNRP1 in the aqueous of patients with treatment-naïve (UnTx) nvAMD compared to non-AMD controls. (**G**) *Above*, Schematic of Laser CNV model in which a single dose of rhsNRP1 control is administered by intravitreal injection 3 days after laser treatment; eyes were enucleated for analysis on day 7. *Below*, size of CNV lesion in mice treated with PBS or rhsNRP1. n = 3-6 animals. Scale bars = 100 μm for G. One-way ANOVA with Bonferroni correction (C and E) and Student's t test (F and G), *P < 0.05; **P < 0.01; ***P < 0.001; ****P < 0.0001; NS, non-significant.

Figure 9

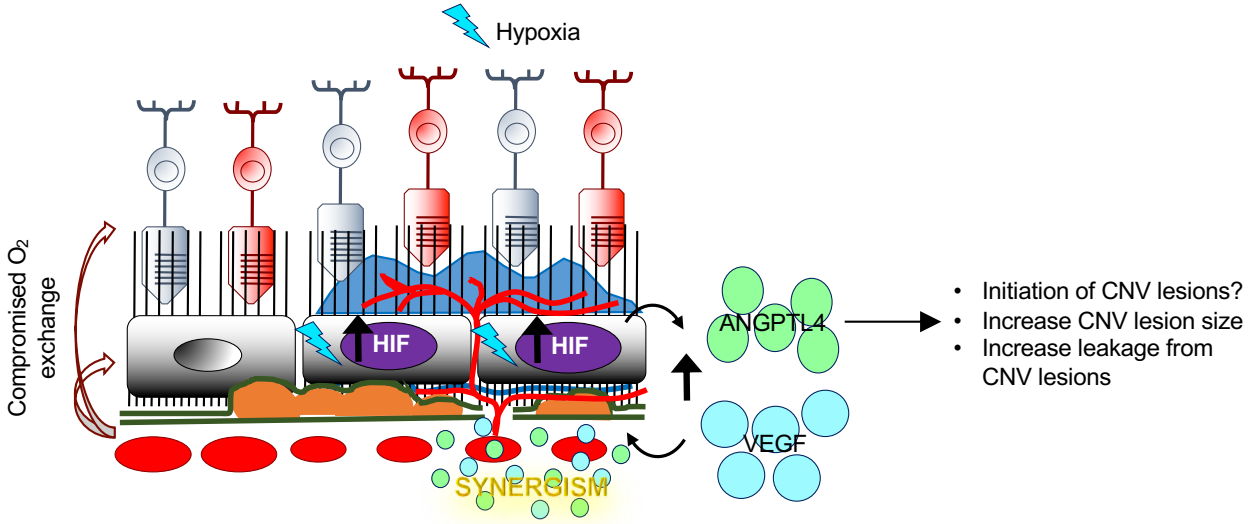
Hypoxia
Compromised O_2 exchange
HIF
HIF
ANGPTL4
VEGF
SYNERGISM
• Initiation of CNV lesions?
• Increase CNV lesion size
• Increase leakage from CNV lesions

Figure 9: Schematic demonstrating the synergistic contribution of VEGF and ANGPTL4 in the development of CNV in patients with nvAMD. In the aging eyes of patients with AMD, collapse of the choriocapillaris combined with thickening of Bruch's membrane and drusen deposits impedes delivery of oxygen to the overlying RPE. This, in turn, results in relative ischemia, the accumulation of HIF-1α, and increased expression of VEGF and ANGPTL4. VEGF and ANGPTL4 cooperate to promote the development of CNV.

Supplemental Tables

Supplemental Table 1. Baseline characteristics of TEP/M and Control patients whose aqueous samples were used for ELISAs.

Characteristic	q4 (n=10)	q6-8 (n=9)	q10-12 (n=6)	Weaned (n=13)	Control (n=39)
Mean Age (yr)	76.2 ± 1.6	78.6 ± 3.0	81.2 ± 1.9	82.5 ± 2.4	70.0 ± 1.5
Female % (#)	60% (6)	56% (5)	83% (5)	77% (10)	56% (22)
Pseudophakic % (#)	90% (9)	89% (8)	33% (2)	85% (11)	23% (9)

Abbreviation: n, sample size; yr, years; q4, TEP/M patients who required treatment with anti-VEGF therapy every 4 weeks at the end of their first year of treatment; q6-8, TEP/M patients who required treatment with anti-VEGF therapy every 6-8 weeks at the end of their first year of treatment; q10-12, TEP/M patients who required treatment with anti-VEGF therapy every 10-12 weeks at the end of their first year of treatment weeks; Weaned, TEP/M patients who were weaned off treatment with anti-VEGF therapy for 30 weeks or longer at the end of their first year of treatment; and ELISA, enzyme-linked immunoassay. Values displayed as mean ± standard error of the mean.

Supplemental Table 2. Performance characteristics of each angiogenic mediator alone and in combination when used to predict patients who were likely to require continuous monthly treatment vs those who required intermittent treatment and those who were able to be weaned.

Angiogenic Factor	Sensitivity	Specificity	AUC
VEGF	0.833	0.529	0.696
ANGPTL4	0.909	0.679	0.802
ANGPT2	0.714	0.454	0.513
VEGF + ANGPT2	0.595	0.743	-
VEGF + ANGPTL4	0.758	0.849	-
ANGPTL4 + ANGPT2	0.649	0.825	-

Abbreviations: AUC, area under curve; VEGF, vascular endothelial growth factor; ANGPTL4, angiopoietin-like 4; ANGPT2, angiopoietin 2.

Supplemental Table 3. Patient Characteristics for aqueous samples.

Patient Characteristic	Control (N=38)	nnvAMD (N=12)	nvAMD Untreated (N=20)	nvAMD Recurrent (N=20)	nvAMD First Treatment§ (N=12)	*P*
Mean Age in Years ± SD	65.6 ± 11.8	76.1 ± 5.7	81.0 ± 5.5	80.6 ± 10.6	78.1 ± 6.6	<0.0001
Males – no. (%)	18 (47)	5 (42)	5 (25)	5 (25)	6 (50)	0.28
Pseudophakic – no. (%)	0 (0)	0 (0)	16 (80)	13 (65)	7 (58)	<0.0001
Prior vitrectomy – no. (%)	0 (0)	0 (0)	0 (0)	0 (0)	0 (0)	–
DM – no. (%)	0 (0)	3 (25)	5 (25)	4 (20)	5 (42)	0.005
CVD[a] – no. (%)	27 (71)	7 (58)	17 (85)	19 (95)	10 (83)	0.09

nnvAMD, non-neovascular age-related macular degeneration. nvAMD, neovascular age-related macular degeneration. DM, diabetes mellitus. CVD, cardiovascular disease.
§Includes unique samples from the same eyes of 8 patients from the nvAMD untreated group.
[a]Includes any patient with a history of hypertension, hypercholesterolemia, coronary artery disease, or cerebral vascular accident.

Supplemental Table 4. Primer sequences for Real-Time (RT)-PCR

	Gene		Sequence (5'to 3')
Mouse			
	Angptl4	Forward	TTGGTACCTGTAGCCATTCC
		Reverse	GAGGCTAAGAGGCTGCTGTA
	Vegf	Forward	CTTATACAGGAATGGAGGCTGT
		Reverse	TTCACCTGACAGGATTGGATAAT
	PPIA	Forward	AGCATACAGGTCCTGGCATC
		Reverse	TTCACCTTCCCAAAGACCAC
	Hif1a	Forward	GCACGGGCCATATTCATGTC
		Reverse	CACGTCATGGGTGGTTTCTTG

Supplemental Table 5. Antibodies used in this study.

Name	Company	Species	Catalog Number	dilution	Marker or Applications
HIF-1α	Gene Tex	rabbit	GTX127309	1:200 or 1:1000	WB
HIF-1α	Novus	mouse	NB-100-105	1:500	IF
HIF-1α	abcam	rabbit	Ab2185	1:500	IHC
β-Actin	Cell signaling	rabbit	4967	1:5000	WB
GAPDH	sigma	mouse	G8795	1:10000	WB
Isolectin GS IB4	Thermo Fisher		I21413	1:200	IF
CD31	R&D	goat	AF3628	1:1000	IF
VEGF	Santa Cruz	rabbit	Sc-152	1:1000	IHC/IF
ANGPTL4	abcam	rabbit	Ab115798	1:400	IHC/IF
Nrp1	abcam	Rabbit	Ab81321	1:1000	WB
Nrp2	Santa Cruz	Mouse	Sc13117	1:1000	WB
2° antibodies	Invitrogen			1:1000	IF
2° antibodies	Dako			1:100	IHC

Supplemental Figure 1

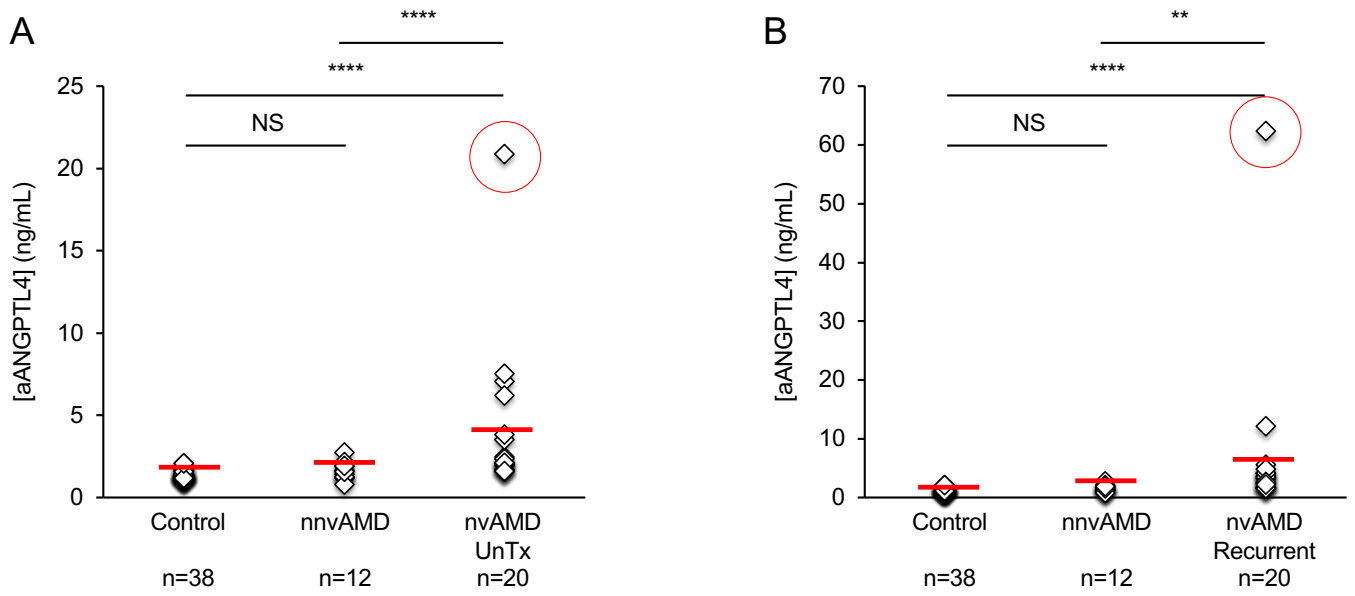

Supplemental Figure 1. Expression of ANGPTL4 in patients with nvAMD.

(**A** and **B**) Aqueous levels of ANGPTL4 in treatment-naïve patients with active nvAMD (i.e., nvAMD patients who have never received anti-VEGF therapy; nvAMD UnTx; A) or patients with nvAMD previously treated with anti-VEGF therapy 12 or more weeks prior to sample collection (nvAMD Recurrent; B) compared to patients with nvAMD and non-AMD (Control) patients. NOTE: Red circle identifies patient sample not displayed in Figure 3B to adequately demonstrate the variability within the nvAMD samples. Kruskal-Wallis with Dunn's multiple comparisons test, *P < 0.05; **P < 0.01; ***P < 0.001; ****P < 0.0001. NS, not significant.

Supplemental Figure 2

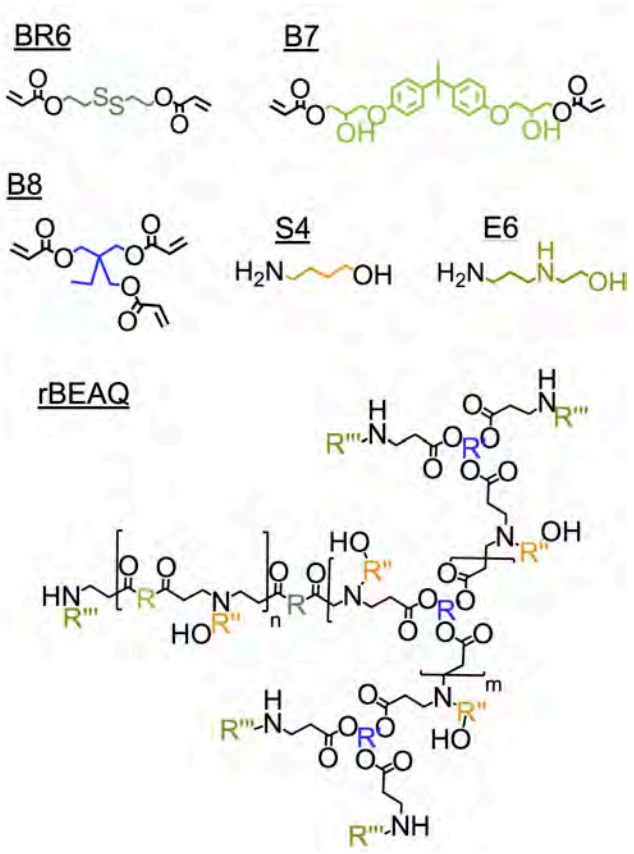

Supplemental Figure 2. Chemical structure of rBEAQ polymer for *in vivo* delivery of siRNA.

Chemical structures for R groups of rBEAQ polymer.